Structural and electronic properties of graphitic nanowiggles

Eduardo Costa Girão, Eduardo Cruz-Silva, Liangbo Liang, Antônio Gomes Souza Filho, and Vincent Meunier

Phys. Rev. B **85**, 235431 — Published 13 June 2012

DOI: 10.1103/PhysRevB.85.235431

Structural and electronic properties of graphitic nanowiggles

Eduardo Costa Girão,[1,2] Eduardo Cruz-Silva,[3,4] Liangbo Liang,[4] Antônio Gomes Souza Filho,[2] and Vincent Meunier[4]

[1] *Departamento de Física, Universidade Federal do Piauí, CEP 64049-550, Teresina, Piauí, Brazil*
[2] *Departamento de Física, Universidade Federal do Ceará, P. O. Box 6030, CEP 60455-900, Fortaleza, Ceará, Brazil*
[3] *Department of Polymer Science and Engineering, University of Massachusetts, Amherst, Massachusetts 01003, USA*
[4] *Department of Physics, Applied Physics, and Astronomy, Rensselaer Polytechnic Institute, Troy, New York 12180, USA*

(Dated: May 10, 2012)

Recent experiments have demonstrated a viable bottom-up strategy to produce narrow and highly ordered nanoribbons, including complex segmented structures called graphitic nanowiggles (GNWs). These defect-free systems are made of successive repetitions of finite-sized graphitic nanoribbons (GNRs) regularly connected at a given angle. Theoretical calculations have shown that these systems exhibit emergent and versatile properties at a level even higher than that found in their basic GNR constituents. Their main structural characteristic is the presence of multiple edge-dependent domains. This atomic structure has a marked influence on their physical properties since GNWs with at least one zigzag sector were shown to accommodate multiple magnetic states. The present detailed study shows how these properties vary with the details of the geometry. We also provide a quantum mechanics based explanation for the origin of GNW's multiple magnetic states. We find that the electronic structure of a GNW is sensitively dependent on the specific way its basic sectors are assembled, as well as on the details of the spin alignment along its edges. As a result, GNWs provide a new means to tune and design systems with desired electronic structure.

I. INTRODUCTION

sp^2 carbon based materials are often regarded as potential candidates to replace silicon in the further scaling down of the size of operational devices. This is due both to the possibility of a broad set of different structural forms and to their unique physical and chemical properties. For instance, graphene-like systems have attracted much attention since the experimental isolation and characterization of a single graphene sheet in 2004[1]. However, the atomically precised synthesis of such nanostructures is a key challenge for experimentalists[2,3] and, in this quest, the efforts of several groups[3–16] have provided significant improvement in the controlled synthesis of flat, one-dimensional carbon nanostructures with size and atomic structure gradually closer to "ideal" systems, as studied theoretically[17–25]. As graphene and related systems have been extensively studied using a variety of theoretical methods, the problem of experimentally assembling basic small-scale components into hierarchical and useful structures has been addressed by both top-down[3–11] and bottom-up[12–16] approaches. The former has been demonstrated for small systems using etching methods on larger-scale graphene substrate[6,26]. The latter is based on self-assembly and preprogrammed chemistry on surfaces involving small molecular building blocks assembled into high-quality samples[3].

Bottom-up synthesis approaches are evolving at a rapid pace and state-of-the-art characterization techniques have highlighted the quality of the samples obtained by chemical routes. In addition, theoretical predictions, aided by ever growing computational capabilities, are successfully predicting a rich array of physical properties that in turn have guided and inspired experimentalists for designing new systems and validating those predictions. This includes electronic structure and thermoelectric transport properties[27,28] and magnetic behaviors[17,19,25,29–32]. More importantly, computational modeling has demonstrated that most of the properties of defect free systems can be fine tuned by well-targeted modifications of the atomic structure, either by introducing local lattice reconstructions or by chemical doping[17–19,21,22,33–38]. Such modifications are particularly effective when they are operated at the edges of the structure[20,23–25,32,39], where the atoms have higher energies. These are just a few examples of the power of theoretical modeling as a fundamental tool for the development of nanotechnology. Of course, hypothetical nanostructures proposed theoretically are often deemed unrealistic, but the recent achievements in the synthesis of exotic low-dimensional systems indicate that actual samples can be built with increasing complexity, thereby improving further the close integration of experiment and theory. A fascinating example is provided by the work of R. Fasel's group[16], who developed an elegant route for the synthesis of narrow and pristine graphitic ribbons. In addition to the well studied straight carbon nanoribbons (GNRs), this type of sample preparation also produces a new type of graphitic ribbons with segmented edge geometry, as well as more complex multi-terminal junctions, depending on the molecular precursor used for the surface-assisted chemical reaction. Different from other methods used for producing nanoribbons, Fasel's method is scalable and produces crystalline edges.

In a recent letter[25] we employed large-scale atomistic modeling to reveal the emergence of unusually attractive properties of the chevrons synthesized in Ref. 16. Because the structures have, in general, a wiggly form rather than a chevron, the name "graphitic nanowiggles" (GNWs) was introduced to refer to them. Due to their rich geometry, GNWs present a broader set of electronic and magnetic properties compared with those of GNRs. This behavior is a result of the intricate GNW structure and edge geometry which define a set of multiple domains along the GNW edge, allowing the formation of a larger number of dissimilar spin distributions compared to GNRs[25]. Similar to a GNR, the ground state of a GNW with at least one zigzag edge presents an anti-ferromagnetic (AFM) spin distribution with local ferromagnetic ordering along the zigzag edges and compatible with the bipartition of the graphene lattice. A systematic study (supported by previous density functional theory calculations[25]) based on a tight-binding+Hubbard (TBU)[40] approach established a general trend for the variation of the GNW's electronic band-gap as a function of the structural parameters in the AFM state. Here we expand the study to other possible (metastable) magnetic states, highlighting specific aspects of the GNW's electronic structure and providing details for shedding light on the origin of the unusual properties.

The rest of this paper is organized as follows. In the next section we describe the theoretical methods used in this study. Section III includes the general framework to determine the atomic structure of GNWs from a reduced set of parameters. The following sections are devoted to discussing the multiple magnetic states in GNWs as well as the systematic studies of the electronic properties for each of the three classes of GNWs containing at least one zigzag edged sector. We then wrap up the paper with our conclusions.

II. METHODS

Tight-binding calculations are known to provide a good description of the electronic properties of carbon based materials[41,42], especially for geometries with moderate to low curvature. Given the size and the number of systems studied in this work, we employed such description to model the GNW's Hamiltonian. Here we restrict the (orthogonal) basis to the $\pi-$orbital and the interactions are accounted up to 3^{rd} neighbors. This $\pi-$orbital description implicitly

considers that carbon atoms on the edges are saturated with hydrogens. We used the parametrization proposed in Ref. 43, so that $\gamma_1 = 3.2$ eV, $\gamma_2 = 0$ eV and $\gamma_3 = 0.3$ eV for the first-, second-, and third-nearest neighbor hopping integrals, respectively, as illustrated in Fig. 1. The different chemical environment at the edges is accounted for by including a $\Delta\gamma_1 = 0.2$ eV correction to the γ_1 parameter for the frontier atoms[43]. The accuracy of this model was previously demonstrated to yield a quantitative agreement with more computationally demanding DFT calculations[25,43].

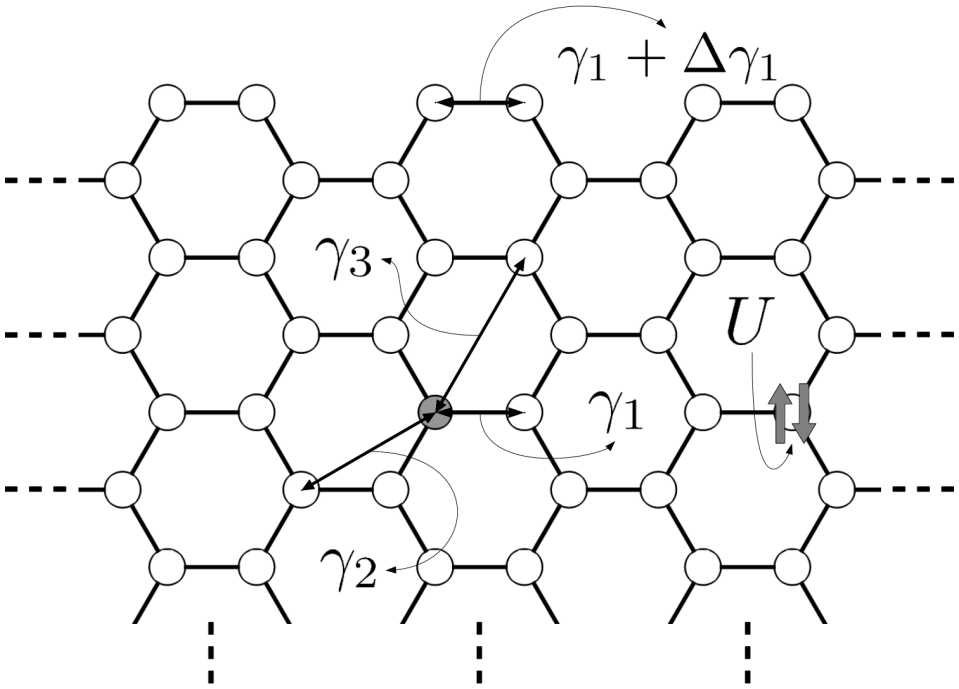

FIG. 1. Schematic representation of the first-, second-, and third-nearest neighbor hopping integrals (γ_1, γ_2 and γ_3, respectively) on an armchair edged graphitic structure. The different chemical environment at the edges is accounted for by a modified first neighbor interaction for these frontier atoms.

While spin-orbit and hyperfine couplings are weak in light elements such as carbon[40,44,45], it is known that non-spin-polarized zigzag edges in graphene present an unstable high charge density which can be resolved by electronic charge polarization[17]. It turns out that the description and understanding of the physics of edge states is fundamental to the successful development of nanodevices based on carbon nanoribbons as they can play a dominant role not only in infinite crystalline systems[17–19], but also in small finite sized structures[31,46,47]. Despite having a lower extent, such border effects persist in long one-dimensional systems even for lengths longer than 70nm[46]. Because of this, a correct description of zigzag edges in graphene should take spin interactions into account.

Adding a Hubbard-like term to the Hamiltonian has been successfully applied to describe the most relevant physical aspects of magnetic states in a number of graphitic carbon nanostructures, including finite nanoislands[29], where the results are shown to be consistent with Lieb's theorem[48]. Fundamental aspects of defect-induced magnetism in graphene and GNRs[34] as well as the magnetic states of zigzag edged GNRs[17,30,40] are also captured by such a simple approach.

The Hubbard Hamiltonian $\hat{H}_U$ is written in terms of the number operators $\hat{n}_i^{\uparrow}$ and $\hat{n}_i^{\downarrow}$ for the spin-orbitals from atom i as

$$\hat{H}_U = U \sum_i \hat{n}_i^{\uparrow} \hat{n}_i^{\downarrow}, \tag{1}$$

where the single parameter U corresponds to the on-site repulsion. Due to the complexity of the 2 body problem, this Hamiltonian is here written as a mean-field interaction:

$$\hat{H}_U = U \sum_i \left(\langle \hat{n}_i^{\uparrow} \rangle \hat{n}_i^{\downarrow} + \hat{n}_i^{\uparrow} \langle \hat{n}_i^{\downarrow} \rangle \right) \tag{2}$$

where the densities $\langle \hat{n}_i^{\uparrow} \rangle$ and $\langle \hat{n}_i^{\downarrow} \rangle$ are determined self-consistently. Here we use $U = 0.92\gamma_1$ as determined from DFT calculations reported in Ref. 25.

Once using a description based solely on the π-orbitals, the TB and Hubbard Hamiltonians can be written, respectively, as

$$\hat{H}_0 = \sum_i \sum_\sigma |i,\sigma\rangle \epsilon_i \langle i,\sigma| + \sum_i \sum_j \sum_\sigma |i,\sigma\rangle \gamma_{i,j} \langle j,\sigma| \tag{3}$$

$$\hat{H}' = U \sum_i \sum_\sigma \langle n_i^\sigma \rangle |i,\bar{\sigma}\rangle \langle i,\bar{\sigma}| \tag{4}$$

where the ket $|i,\sigma\rangle$ represents an orbital centered on the i-th orbital from the structure and having spin σ (which can be either $\uparrow$ or $\downarrow$) and $\bar{\sigma}$ is the spin orientation opposite to σ. In addition, ϵ_i is the site energy and γ_{ij} is the hopping parameter between orbitals i and j (which is zero unless the orbitals correspond to first-, second- or third-neighbor atoms). Writing these Hamiltonians in terms of Bloch functions based on the π-orbitals results in:

$$H(\mathbf{k}) = \begin{bmatrix} H_0(\mathbf{k}) & 0 \\ 0 & H_0(\mathbf{k}) \end{bmatrix} + \begin{bmatrix} H^\uparrow & 0 \\ 0 & H^\downarrow \end{bmatrix} \tag{5}$$

where $H_0(\mathbf{k})$ is the usual TB matrix having elements:

$$[H_0(\mathbf{k})]_{ij} = \epsilon_i \delta_{ij} + \sum_{j'} \gamma_{ij'} e^{i\mathbf{k}\cdot\mathbf{R}_{j'}} \tag{6}$$

with i and j being in a given unit cell, the sum in j' being over all the sites equivalent to j through a Bravais lattice translation $\mathbf{R}_{j'}$ and $\mathbf{k}$ a vector within the first Brillouin zone (BZ). On the other hand, the Hubbard matrices elements are written as:

$$[H^\sigma]_{ij} = U \langle n_i^{\bar{\sigma}} \rangle \delta_{ij} \tag{7}$$

The eigenvectors $c(\alpha,\mathbf{k})$ (where α labels the bands) and eigenvalues $E_\alpha(\mathbf{k})$ are then obtained from the secular equation:

$$[E_\alpha(\mathbf{k}) \cdot I - H] \cdot c(\alpha,\mathbf{k}) = 0 \tag{8}$$

where I and 0 are, respectively, the identity and zero matrices and the elements of the column vectors $c(\alpha,\mathbf{k})$ are $c_{i,\sigma}(\mathbf{k},\alpha)$. Numerically diagonalizing the Hamiltonian is straightforward with well-know routines[49]. The densities $\langle n_i^{\bar{\sigma}} \rangle$ can be obtained from the eigenvectors by:

$$\langle n_i^\sigma \rangle = \frac{1}{v_{BZ}} \int_{\mathrm{BZ}} \left(\sum_\alpha f(E_\alpha) |c_{i,\sigma}(\mathbf{k},\alpha)|^2 \right) d\mathbf{k} \tag{9}$$

where $f(E_\alpha)$ is the Fermi distribution and v_{BZ} the volume of the BZ. Such densities are obtained within a self-consistency cycle where we used a Pulay mixing to accelerate convergence[50].

III. ATOMIC STRUCTURE OF GNWS

GNWs are one-dimensional crystals made up of successive repetitions of parallel and oblique GNR domains (Fig. 2). Experimentally, GNWs are built from smaller molecules, but geometrically, it may be simpler to use individual GNRs as a basis to describe them. Their GNR building blocks are seamlessly stitched together without the need of structural defects, such as pentagons, heptagons, or higher order cycles. If we restrict possible geometries to achiral GNWs, we can denote the parallel and oblique sectors by P_α and O_β, respectively, with $\alpha,\beta = A, Z$ depending on the type of sector (armchair (A) or zigzag (Z)). The possible combinations are therefore: armchair-armchair (AA-GNW), armchair-zigzag (AZ-GNW), zigzag-armchair (ZA-GNW) and zigzag-zigzag (ZZ-GNW) geometries, named after the parallel and oblique edges, respectively, as shown in Fig. 2.

Alternatively, GNWs can be conceptualized as armchair or zigzag GNRs from which trapezoidal wedges are carved out on alternating edges as depicted by shaded areas for the four achiral GNW types in Fig. 2. We observe that the non-parallel sides of the trapezoidal wedges make an angle of 60° (30°) with the GNW's periodic direction if $\alpha = \beta$ ($\alpha \neq \beta$). Here we do not consider the limiting case in which the trapezoid becomes a rectangle (90°). In addition, we consider only systems with a vertical symmetry mirror σ_v perpendicular to the wiggle's plane.

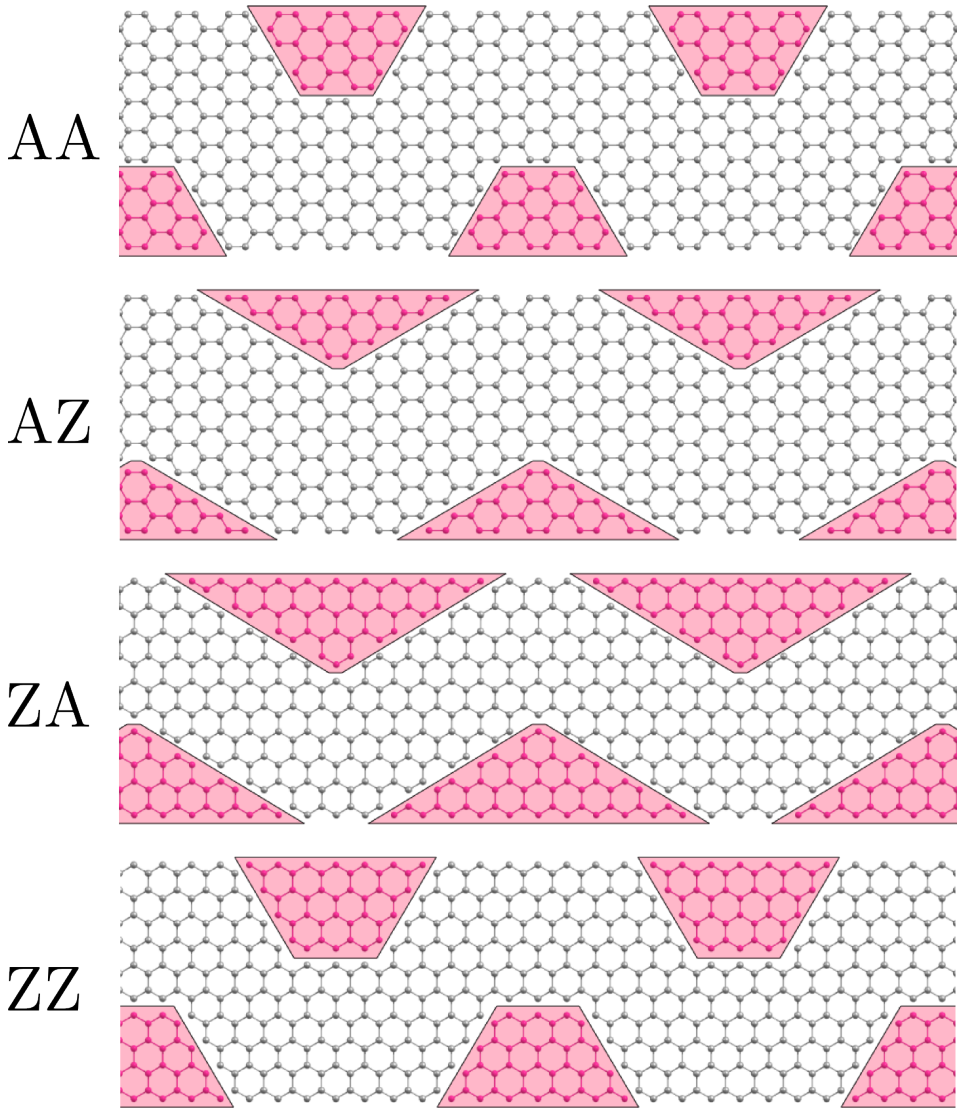

FIG. 2. (color online) The four achiral GNW types and schematic construction of the structures: initial GNR and the trapezoidal wedges needed to be removed to transform it into a GNW. The four structures are Armchair-Armchair (AA-GNW), Armchair-Zigzag (AZ-GNW), Zigzag-Armchair (ZA-GNW) and Zigzag-Zigzag (ZZ-GNW), depending on the edge geometry for the parallel and oblique sectors, respectively.

A. Geometrical parameters

An arbitrary GNW is characterized by four parameters, introduced in Fig. 3. Two parameters, W_p and W_o, are the number of C-C bonds (for armchair sectors) or zigzag strips (for zigzag sectors) along the width of the parallel and oblique sectors, respectively. These two parameters are illustrated for an AZ-GNW in Fig. 3a. The other two parameters, L_p and L_o provide the length of the parallel and oblique sectors. L_o is the number of $C-C$ lines or zigzag strips along the width of the wedge-healed GNW (similarly to the definition of W_p and W_o). L_p is expressed in units of the $C-C$ distance in graphene a_{CC} for AA- and AZ-GNWs (as illustrated in Fig. 3b). L_p is the number of zigzag tips (carbon atoms having only two carbon atoms as first neighbors) expanding along the smallest basis of the trapezoid formed by the edge atoms for ZA- and ZZ-GNWs (as shown in Fig. 3c). With the set of four parameters $(W_p, W_o) - (L_p, L_o)$ the GNW structure is uniquely defined. In this work, we will restrict the values of L_p and L_o so that L_p is the smallest possible and L_o is such that at least one $C-C$ line or zigzag strip (along the GNW's length) is not interrupted by the wedges. Imposing this condition leads to a general notation $(P_\alpha, O_\beta) = (W_p, W_o)$ for any achiral GNW (where α and β can be either A for armchair or Z for zigzag sectors) while the other two parameters are constants implicitly given by $L_p = 2$ (for AA- and AZ-GNWs) or $L_p = 1$ (for ZZ- and ZA-GNWs) and L_o being

the greatest allowed integer (see restrictions in Section III B) such that $L_o \leq 2W_p - 1$.

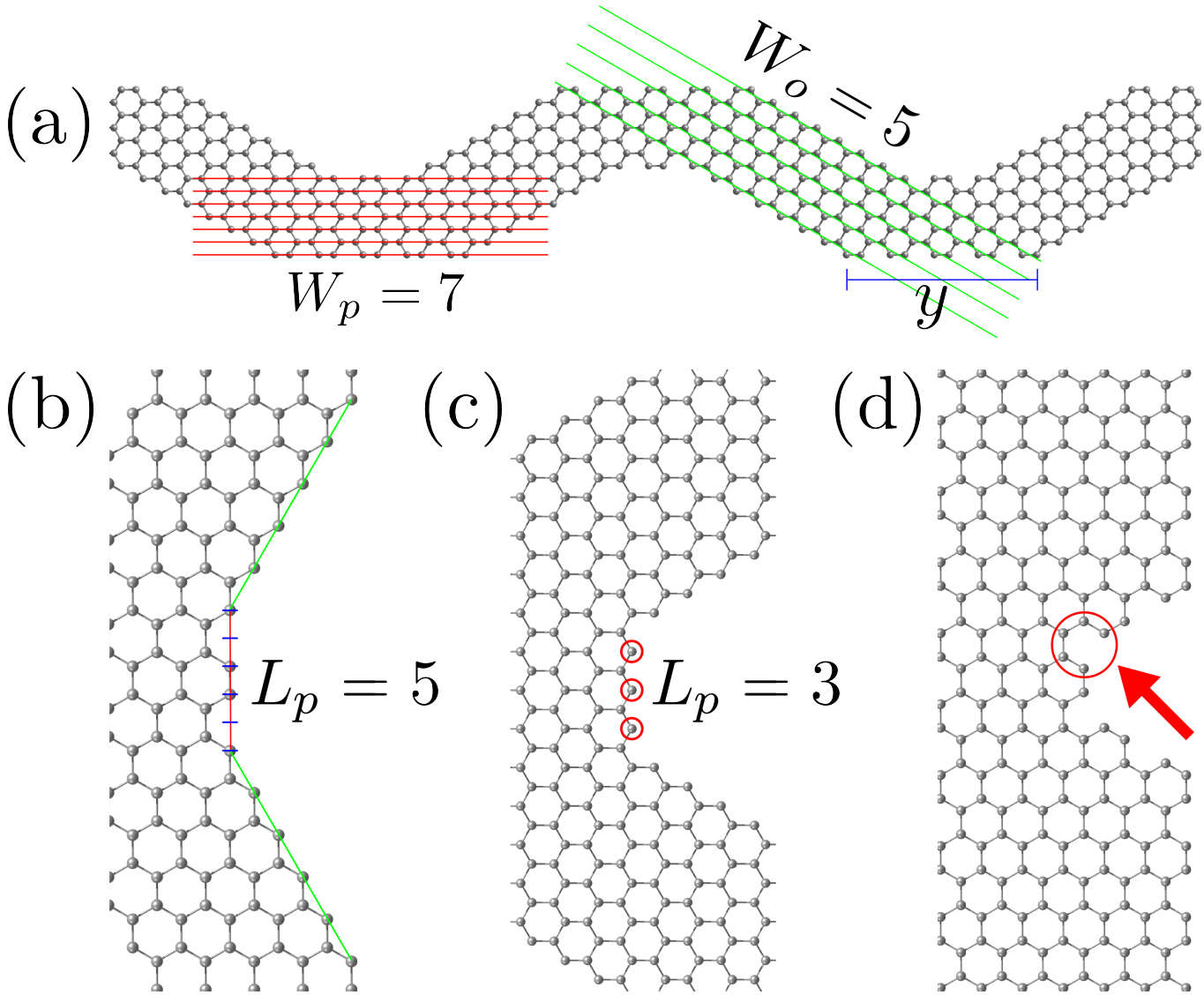

FIG. 3. (color online) (a) Definition of the W_p and W_o parameters as the number of $C - C$ lines or zigzag strips along the width of each sector and the length y of the outer edge of the parallel sector. Here the example of an AZ-GNW with $W_p = 7$ (red lines) and $W_o = 5$ (green lines). (b-c) Definition of the parameter L_p as the number of a_{CC} lengths (AA- and AZ-GNWs) or zigzag tips (ZA- and ZZ-GNWs, where a tip is a carbon atom having only two carbons as neighbors) along the smallest basis of the trapezoid formed by the GNW's edge atoms. Here the example of an AZ-GNW with $L_p = 5$ (b) and a ZZ-GNW with $L_p = 3$ (c). (d) AA-GNW structure not allowed by the $L_p \neq 3i$ condition.

All the important GNW structural properties are uniquely determined by these four parameters. For example, the lattice parameter $\mathcal{L}$ is given by the following equations (see Appendix A):

$$\mathcal{L}_{AA} = (2W_o + L_o + 2L_p - 2W_p - 1)a_{CC}; \tag{10}$$
$$\mathcal{L}_{AZ} = (6W_o + 3L_o + 2L_p - 6W_p - 1)a_{CC}; \tag{11}$$
$$\mathcal{L}_{ZA} = (2W_o + 3L_o + 2L_p - 6W_p - 2)a_{CC}\sqrt{3}; \tag{12}$$
$$\mathcal{L}_{ZZ} = (2W_o + L_o + 2L_p - 2W_p)a_{CC}\sqrt{3}. \tag{13}$$

The number of atoms ($\mathcal{N}$) contained within a unit cell is also a function of L_p, W_p, W_o and L_o (see Appendix B):

$$\mathcal{N}_{ZZ} = 4W_oL_o + 4L_pW_p - 2W_p^2; \tag{14}$$
$$\mathcal{N}_{ZA} = 4W_oL_o + 4L_pW_p - 6W_p^2 - 4W_p; \tag{15}$$

$$\mathcal{N}_{AZ} = (12W_oL_o + 4L_pW_p - 6W_p^2 - 2W_p)/3; \tag{16}$$

$$\mathcal{N}_{AA} = (4W_oL_o + 4L_pW_p - 2W_p^2 - 2W_p + \tau)/3 - \tau', \tag{17}$$

where the value of τ and τ' for AA-GNWs is given by:

$$\tau = \begin{cases} 0 & \text{if } [p;q] = [1;0],[1;2],[2;0] \\ -4 & \text{if } [p;q] = [2;1],[2;2] \\ 4 & \text{if } [p;q] = [1;1] \end{cases}, \quad \tau' = \begin{cases} 4 & \text{if } [p;q] = [2;2],[1;0] \\ 0 & \text{otherwise} \end{cases}, \tag{18}$$

with $p = mod(L_p, 3)$ and $q = mod(L_o - W_p, 3)$. As we will show below, the cases where $mod(L_p, 3) = 0$ are not possible, due to the unstable chemical environment that this choice would create at the edges.

B. Geometrical restrictions

We should stress that although any GNW is uniquely defined by a set of four parameters W_p, W_o, L_p and L_o, it is not true that any set of four numbers corresponds to a valid GNW. We will now discuss the corresponding formal restrictions to apply to these parameters.

First, for all the four groups of achiral GNWs we must have:

$$W_o, W_p \geq W^{min}; \qquad L_o \geq W_p \qquad \text{and} \qquad L_p \geq L_p^{min}. \tag{19}$$

The first restriction represents the lower limit where either the parallel or oblique sector becomes a polyacetylene chain ($W^{min} = 2$ (1) for A (Z) sectors) and the second one ensures that the oblique length is not smaller than the width from the GNR making up the wiggle. The L_p^{min} parameter is the minimum length for the inner edge of the parallel sector such that edges from successive oblique sectors do not touch one-another (with $L_p^{min} = 2$ for AA- and AZ-GNWs and $L_p^{min} = 1$ for ZZ- and ZA-GNWs). Additional specific restrictions apply for each case.

For AA-GNWs, the L_p parameter has to obey $L_p \neq 3j$ (j an integer) in order to avoid rings with only one missing atom, as shown in Fig. 3d. In addition, we are restricted to $L_p = 3j + 2$ for AZ-GNWs, since $L_p = 3j$ denotes the same structure as that given by $L_p = 3j + 2$, while the $2 \leq L_p = 3j + 1$ case would produce a large number of single-bonded carbon atoms.

The specific structure of AA-GNWs imposes an additional condition on $\mathcal{L}_{AA}$ which must be a multiple of $3a_{CC}$. Using the lattice parameter relation from Eq. 10, this restriction takes the form:

$$2W_o + L_o + 2L_p - 2W_p - 1 = 3l \quad \text{(AA-GNWs)} \tag{20}$$

where l is an integer. A similar restriction should also be applied to AZ-GNWs, but the corresponding equation is automatically satisfied since $L_p = 3j + 2$ in this case.

Finally, the length y corresponding to the outer edge of the parallel sector (Fig. 3a) has a specific lower bound value for each GNW type. For AA-GNWs, this value is $y_{min} \times a_{CC}$ with $y_{min} = 3$, $y_{min} = 1$ or $y_{min} = 5$ for $mod(y/a_{CC}, 3) = 0, 1, 2$, respectively, as illustrated in Fig. 4a-c. For AZ-, ZA- and ZZ-GNWs, the minimum value is a_{CC}, 0 and $2a_{CC}\sqrt{3}/3$, respectively, as exemplified in Fig. 4d-f.

After using the expression for y in Appendix A for each GNW class we end up with:

$$AA \quad \rightarrow \quad 2W_o + L_p - W_p - 1 \geq y_{min}; \tag{21}$$

$$AZ \quad \rightarrow \quad 6W_o + L_p - 3W_p \geq 2; \tag{22}$$

$$ZA \quad \rightarrow \quad 2W_o + L_p - 3W_p \geq 1; \tag{23}$$

$$ZZ \quad \rightarrow \quad 2W_o + L_p - W_p \geq 1. \tag{24}$$

IV. ELECTRONIC STRUCTURE AND MULTIPLE MAGNETIC STATES

The general framework presented in Section III to classify and obtain the atomic details of any nanowiggle can be used for the systematic study of their electronic structure. As highlighted in Ref. 25, GNWs are known to present multiple magnetic states (see Fig. 5), with the notable exception of AA-GNWs. The spin polarization in such structures is essentially concentrated along the zigzag edges, where the local ordering is ferromagnetic. The magnetic moment is maximal at the center of the zigzag edges, decaying towards the edge corners[29,31,47,51].

We observe that in all cases, the ground state corresponds to an anti-ferromagnetic (AFM) distribution obeying the bipartition of the graphene lattice (so that each sub-lattice presents a given spin orientation as its majority spin). In

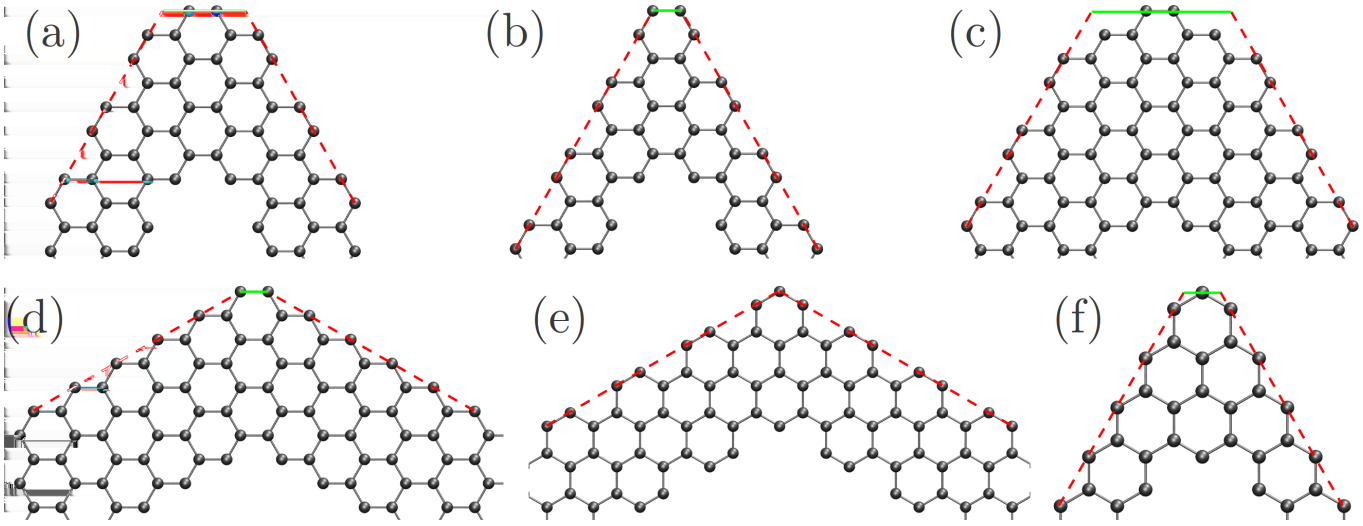

FIG. 4. Examples for the minimum value of the length y of the outer parallel edge (full green lines) in AA- (a-c), AZ- (d), ZA- (e) and ZZ-GNWs (f).

addition to AFM and the trivial paramagnetic distribution (PM, for which there is no spin polarization, in analogy to Z-GNRs[52]), there is also a set of other metastable states for each GNW class. This number of different magnetic states is reduced for ZA-GNWs (when considering the spin distribution along a single unit cell) since we find only a ferromagnetic (FM) state in addition to the AFM and PM cases, similar to Z-GNRs[17]. However, AZ-GNWs also develop two additional states that we called trans-anti-ferromagnetic (TAFM) and longitudinal-anti-ferromagnetic (LAFM) states (depending on the directions along which the edge-to-edge flipping for the majority spin takes place). With the notable exception of the FM distribution, the symmetry of all the spin configurations ensures a zero total magnetization integrated over an entire unit cell. In addition, ZZ-GNWs present AFM, FM, TAFM and PM distributions as well as a longitudinal-ferrimagnetic (LFiM) state. The symmetry of this last distribution does not impose a zero total magnetization for a ZZ-GNW unit cell, similar to the FM state. These spin distributions (except the PM case for which there is no spin polarization) are schematically represented in Fig. 5.

As a consequence of the fact that zigzag edges have to be longer than a threshold value to promote spin polarization[31,51], some pair of magnetic states can be indistinguishable from each other when either a parallel or oblique zigzag sector is short enough to preclude such polarization. These cases will be highlighted in the following sections.

In this work we performed a similar systematic study as in Ref. 25 to determine how the energy gap around the Fermi energy behaves as a function of the GNW's geometry. However, here we do not limit our study to the AFM state, rather we extend it to all the possible spin distributions on AZ-, ZA- and ZZ-GNWs.

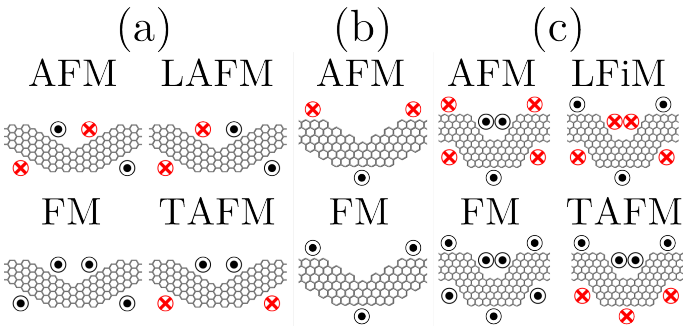

FIG. 5. (color online) Schematic representation of the possible spin distributions in (a) AZ-GNWs, (b) ZA-GNWs and (c) ZZ-GNWs. Circles with a dot or a cross represent majority spin-up or -down, respectively.

In the extended set of systems studied here, the length of both P and O sectors is restricted according to the conditions presented in Section III, while the corresponding widths are varied over a broad range. These calculations are based on the TBU model described in Section II.

In the following we discuss the electronic and magnetic properties of all the three GNW classes containing at least

one zigzag edge.

V. ELECTRONIC STRUCTURE AND MAGNETIC STATES OF AZ-GNWS

A. Electronic band-gap

An AZ-GNW is composed of armchair-edged parallel sectors, while its oblique sectors are zigzag edged. In Fig. 6 we plot the electronic band-gap as a function of P_A and O_Z for the five possible spin distributions in AZ-GNWs. We varied the parallel and oblique widths so that both P_A and O_Z span the range from 5 to 17. The minimum (Δ^{AZ}_{min}) and maximum (Δ^{AZ}_{max}) values for the gap in each spin-configuration are shown in Table I.

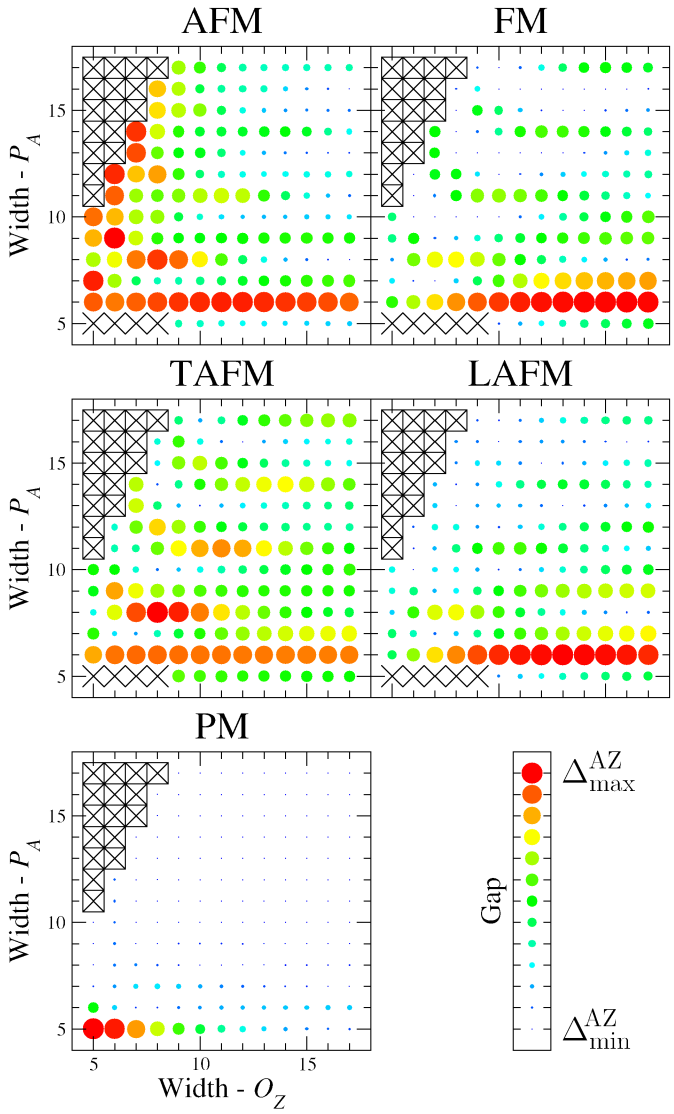

FIG. 6. (color online) Energy band-gap as a function of P and O widths for the multi-magnetic states in AZ-GNWs. Systems that do not possess a stable AFM, TAFM, LAFM or FM distribution of spins are marked by a cross, while points marked with a cross inside a square correspond to geometries not allowed by the particular choice for the lengths of the P and O sectors. The minimum and maximum values for the gap in each plot are shown in Table I.

Data shown in Table I confirm that the AFM state is always semiconducting, while the PM and FM states can assume either a metallic or semiconducting behavior. The other LAFM and TAFM states are never truly metallic at zero temperature, but some structures present very small gaps of only a few meV. We observe from Fig. 6 that with

TABLE I. Minimum (Δ^{AZ}_{min}) and maximum (Δ^{AZ}_{max}) values for the electronic band-gaps in each spin-configuration for AZ-GNWs.

	AFM	TAFM	LAFM	FM	PM
Δ^{AZ}_{min} (meV)	183	22	7	0	0
Δ^{AZ}_{max} (meV)	446	396	428	347	393

the exception of the systems with narrow parallel sectors, the PM state is always metallic. We note that wide parallel sectors produce long O_Z sectors for a given oblique width. It follows that for larger P_A, the AZ-GNWs properties are dominated by the O_Z sector (which, when isolated, are metallic in their PM state), except for the 120° turn made by the Z-GNR sector as it meets the short A-GNR sector. However, the calculations also indicate that the small parallel sector does not affect sufficiently the structure to make it semiconducting in the PM state.

In contrast, the small parallel sector has a much more dramatic effect on the FM and LAFM states. We notice that the P_A sector affects sufficiently the electronic structure to open a gap even for longer oblique sectors (corresponding to wider parallel sectors), which are composed by Z-GNRs in their FM metallic state (see the LAFM and FM spin distributions for AZ-GNWs in Fig. 5a). These aspects related to the non-PM states show that the P_A sector has a critical influence on the AZ-GNWs' electronic properties, even for short parallel sectors. For the LAFM state we have an additional factor to consider, namely the presence of successive FM O_Z sectors, which have alternating spin orientations. This effectively separates the atoms with identical spin orientation to portions far from each other. This arrangement contributes to form localized states that also affect the opening of a band-gap. These findings show that the interplay between A- and Z-GNRs in GNWs is not only restricted to the simple sum of their individual properties, but is in fact sensitively dependent on the specific way these pieces are assembled into the GNW.

The dependence of the electronic band-gap with the atomic structure for non-PM states presents three distinct behaviors corresponding to sector widths P_A such that mod$(P_A, 3)$ =0, 1, or 2. Moving horizontally across the chart, the electronic band-gap oscillates for small O_Z values and gradually converges to a P_A-dependent constant that can be associated with the gap of a pristine A-GNR originating at the wedge-healed GNW (because the GNW structures approach an A-GNR with a sparse distribution of defects as $O_Z \to \infty$ for a fixed P_A).

B. Electronic structure of the FM state

The FM spin distribution is the only one to present a net magnetization integrated over a single AZ-GNW unit cell. As a result of this broken spin-up and -down symmetry, the FM state shows non-spin-degenerate bands. This additional dependence of the electronic structure with the spin allows to use this property to tune the physical properties of AZ-GNWs in this particular spin distribution. Analyzing the electronic structure of this series of structures in their FM state, we classified the general features of the bands close to the Fermi energy into 4 different classes: M, S$\updownarrow\updownarrow$, S$\uparrow\downarrow$ and S$\downarrow\uparrow$. Class M corresponds to metallic structures. The $(10_A, 7_Z)$ GNW whose electronic bands are shown in Fig. 7 (where a spin-up and a spin-down branch cross at E_F) is an example of a M system. The S$\updownarrow\updownarrow$ class corresponds to the semiconducting structures where we have a crossings between spin-up and -down bands right below and above the Fermi energy (see, for instance, the bands for the FM state of the $(8_A, 6_Z)$ structure in Fig. 7). The S$\uparrow\downarrow$ (S$\downarrow\uparrow$) symbol denotes semiconducting structures where the highest band below E_F corresponds to spin-up (-down) and the lowest band above E_F corresponds to spin-down (-up). This is illustrated for the $(7_A, 5_Z)$ and $(7_A, 8_Z)$ ($(8_A, 9_Z)$ and $(8_A, 8_Z)$ structures in Fig. 7.

Figure 8a shows AZ-GNW structures along with the FM class they belong to. One observes that the metallic systems are mostly those with $mod(P_A, 3) = 1$. This contrasts with the properties of the isolated parallel sectors since A-GNRs with $(3i + 1)$ $C - C$ lines (i an integer) along their width possess larger gaps than the corresponding $(3i)$ and $(3i + 2)$ cases. On the other hand, we observe that all the metallic structures are on the $P_A \geq O_Z$ part of the plot. This observation can be explained by the fact that the outer armchair edge from the GNW becomes shorter for narrow O_Z sectors and the electronic properties correspond mainly to the zigzag sectors (which have a tendency to be metallic in the FM state). In addition, the shorter parallel edges favor electronic tunneling between zigzag sectors through the semiconducting armchair sector. Moving to the semiconducting systems, we observe that, for sectors wider than 8, the S$\downarrow\uparrow$ character is favored for parallel sectors where the corresponding A-GNRs have the smallest gaps $mod(P_A, 3) = 2$. For $mod(P_A, 3) = 0, 1$ there is a clear preference for the S$\uparrow\downarrow$ bands.

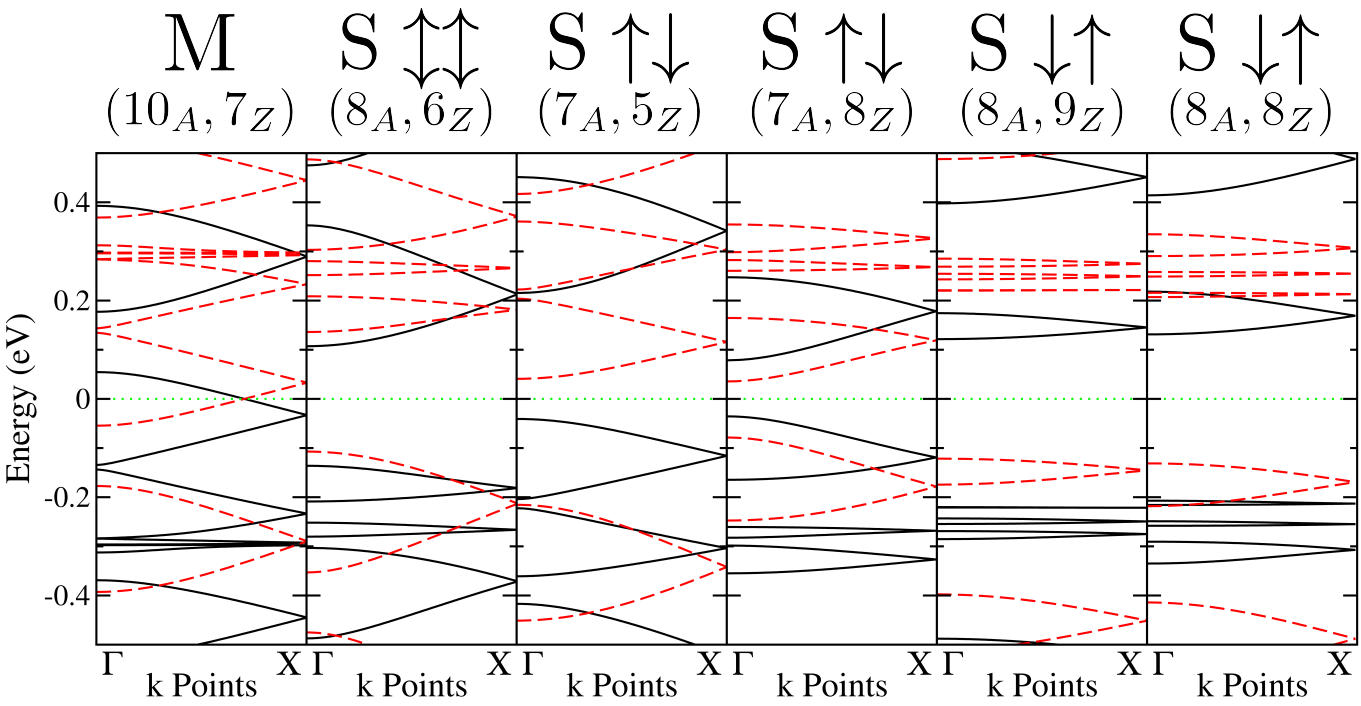

FIG. 7. (color online) Electronic band-structure of some AZ-GNWs in their FM state (spin-up and -down levels are shown in black and red, respectively) and their classification as M, S↕↕, S↑↓ or S↓↑ according to the nature of the bands close to the Fermi energy.

C. Band-structure energy

The TBU band-structure energy method provides a useful qualitative tool to estimate the relative stability of different magnetic states from the same atomic structure[25]. This quantity is numerically computed as:

$$E_{\mathrm{TBU}} = \int_{-\infty}^{E_F} En(E)dE \tag{25}$$

where $n(E) = n_\uparrow(E) + n_\downarrow(E)$ is the total density of states. We computed the difference in the band-structure energy among the different magnetic states for all the structures considered in the gap study. In Fig. 9 we show these energy differences for different pairs of magnetic states as a function of the sector widths.

Among all the pairs of states involving the PM case, we show only the $E_{PM} - E_{AFM}$ difference since the other plots present the same features. From this specific plot in Fig. 9 we see that the energy of the PM state is in general much larger than that of the AFM state (as well as for all the other states). This is remarkable for GNWs with larger parallel width, while narrower P_A sectors give a PM state closer in energy to the other states. As the long zigzag edged sectors correspond to wider P_A sectors, the energy necessary to develop a non-polarized zigzag edge increases. Conversely, as P_A narrows, the edges of the oblique sector shortens and the parallel sector becomes longer, so that the GNW edge structure is predominantly armchair, favoring a paramagnetic distribution for the spin. The $|\Delta E|_{max}$ values for each pair of states are listed in Table II

TABLE II. Maximum values of the band-structure energy difference ($|\Delta E|_{max}$) for the different pairs of magnetic states in AZ-GNWs.

$\lvert\Delta E\rvert_{max}$ (eV)	AFM	TAFM	LAFM	FM
PM	4.995	4.914	4.875	4.799
FM	0.830	0.504	0.478	–
LAFM	0.559	0.476	–	–
TAFM	0.479	–	–	–

All the other magnetic states are closer in energy to each other. As a general trend, we observe that the states

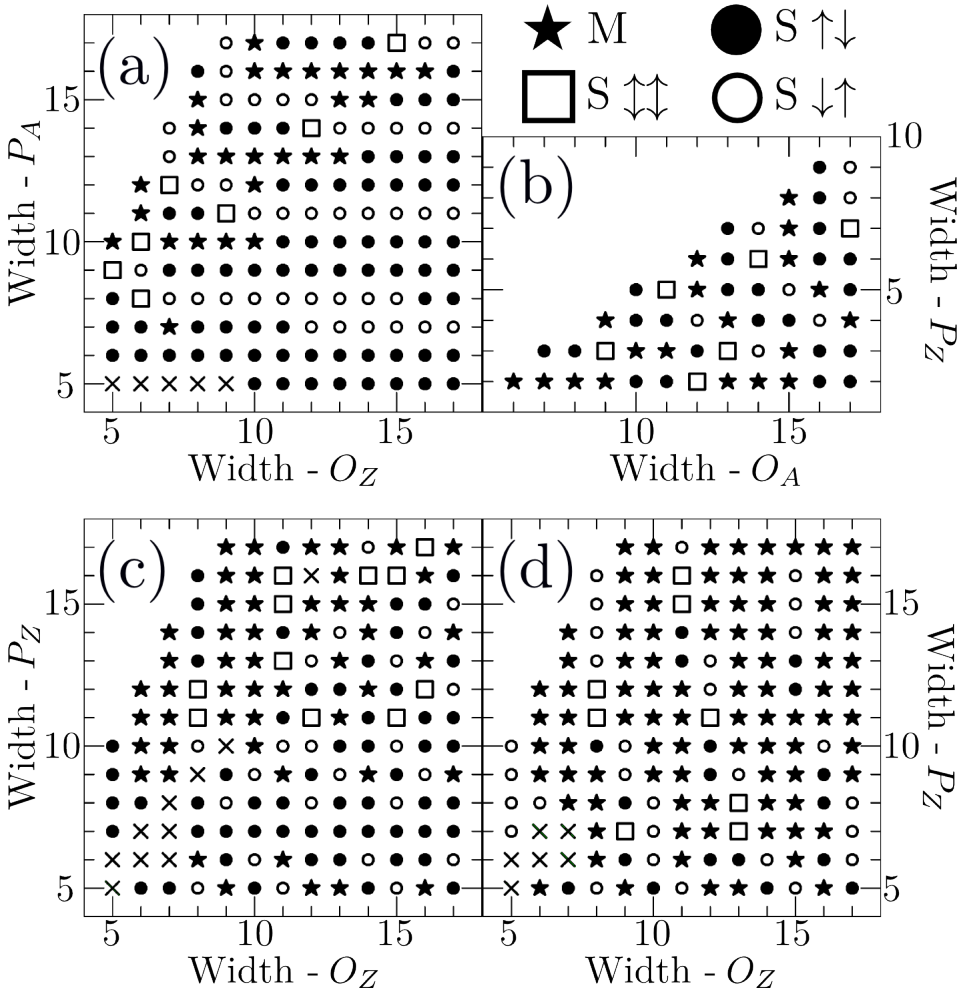

FIG. 8. Determination of the M ($\star$), S$\updownarrow\updownarrow$ ($\square$), S$\uparrow\downarrow$ ($\bullet$) or S$\downarrow\uparrow$ ($\circ$) character for AZ- (a) and ZA-GNWs (b) in their FM state and for ZZ-GNWs in their FM (c) and LFiM (d) states.

obey the following order for increasing TBU energy: AFM < TAFM < LAFM < FM < PM. We do observe some exceptional cases, such as the $(9_A, 7_Z)$ GNW for the LAFM-FM pair and some set of horizontal lines (corresponding to $mod(P_A, 3) = 1$) in the LAFM-TAFM plot. We also observe other set of points in discordance with the energy order above, but these are among the points for which the absolute value of the energy difference is very low (small triangles) and lie within the method's error bar.

Turning to other magnetic states, we note that the energy differences between TAFM and AFM and between FM and LAFM are notably higher for the $mod(P_A, 3) = 1$ family. We can understand this behavior in terms of the spin distributions along the zigzag edges (from the oblique sector) and the properties of the parallel sector. As the occupied (unoccupied) energy bands are pushed down (up) for a semiconducting system, a larger gap is a factor which, in principle, lowers the value of E_{TBU}. Note that in the AFM state, the edges with similar majority spin (edges 1 and 4 or 2 and 3 in Fig. 10a) are more likely to be farther away from each other than in the TAFM distribution (edges 1 and 3 or 2 and 4 in Fig. 10a), as seen in Fig. 10b. In the TAFM state, this contributes to form more extended states (favoring the reduction of the gap). This effect is similar but opposite in the AFM case, thus contributing to a band-gap increase, and in turn to a band-structure energy reduction. Thus, since A-GNRs with a number N of $C-C$ lines along their width have the largest gaps for $mod(N, 3) = 1$, parallel sectors with $mod(P_A, 3) = 1$ are likely to correspond to more stable structures. Our results show that this trend is more pronounced for the AFM state than for the TAFM distribution, leading to a larger TAFM-AFM energy difference. A similar argument can be made for the FM-LAFM difference (see Fig. 10b).

We observe a similar behavior in the LAFM-AFM and FM-TAFM energy differences for systems with $mod(P_A, 3) = 2$. Let us consider edge 1 in Fig. 10a, for instance. Since it is close to edges 2 and 3, we will call 1 and 2 or 1 and 3 as "neighbors". While a zigzag edge with a given spin polarization has one "neighboring" zigzag edge with the

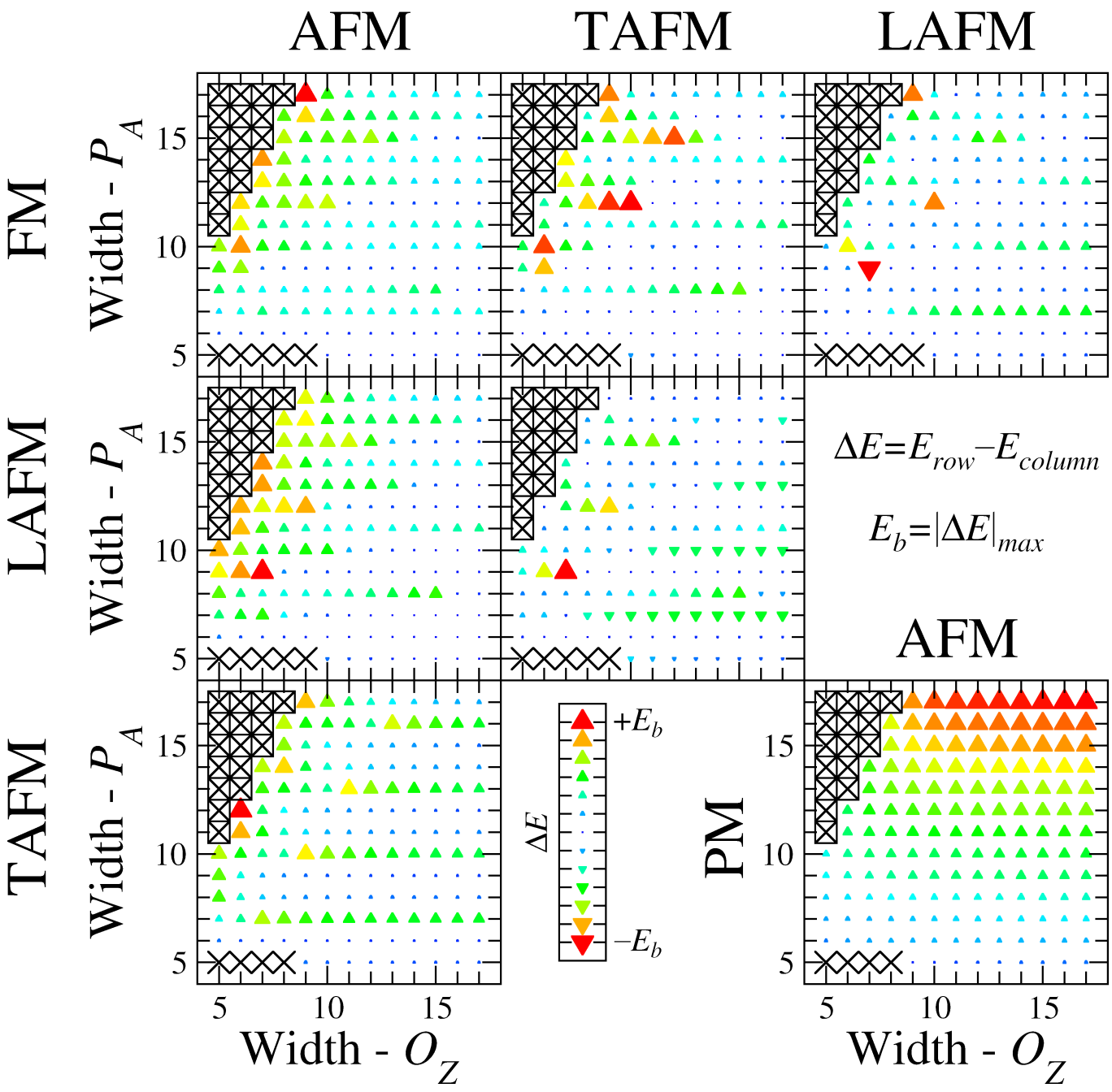

FIG. 9. (color online) Band-structure energy difference among the different magnetic states as a function of P_A and O_Z in AZ-GNWs. Systems that do not possess a stable AFM, TAFM, LAFM or FM distribution of spins are marked by a cross, while points marked with a cross inside a square correspond to geometries not allowed by the particular choice for the lengths of the P and O sectors. The $|\Delta E|_{max}$ values for the different plots are shown in Table II.

same polarization in LAFM, the corresponding edge on the AFM state has no "neighbor" with the same majority spin (see Fig. 10c). Thus, LAFM has a more pronounced tendency to present a smaller gap than AFM. At the same time, A-GNRs with a number N of $C-C$ lines along their width will present the smallest gaps for $mod(N,3)=2$. Consequently, parallel sectors with $mod(P_A,3)=2$ are likely to produce less stable structures, at least on the basis of their band-structure energy. Our results show that this trend is more pronounced for the LAFM state than for the AFM case, thereby accounting for the larger LAFM-AFM energy difference. A similar discussion can be developed to account for the FM-TAFM difference in energy (see Fig. 10c).

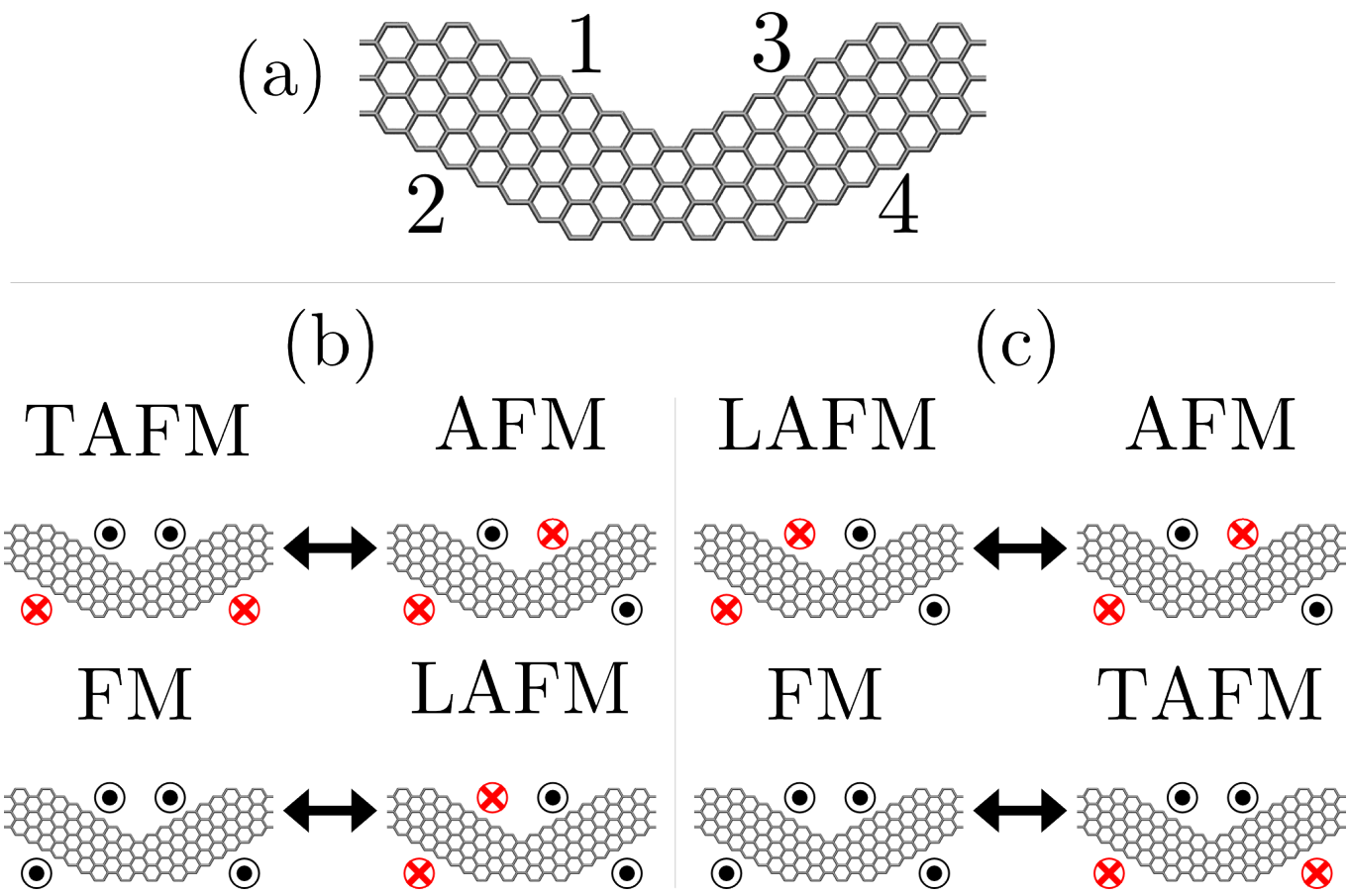

FIG. 10. (color online) Location of the zigzag edges (a) and schematic representation of the pairs of magnetic states which give the largest energy splitting for $mod(P_A, 3) = 1$ (b) and $mod(P_A, 3) = 2$ (c) in AZ-GNWs.

VI. ELECTRONIC STRUCTURE AND MAGNETIC STATES OF ZA-GNWS

A. Electronic band-gap

Compared to the other GNW classes, we notice a reduced set of possible spin distributions on a single unit cell of ZA-GNWs: PM, AFM and FM. These states are similar to those on zigzag edged GNRs. Our systematic study involves structures with sector widths P_Z and O_A varying between 2 and 10; and 6 and 17, respectively. As in the AZ-GNWs case, we observe three families of behaviors for mod$(O_A, 3)$ =0, 1, and 2. As the armchair edges are located at the oblique sector, these families extend along the vertical direction of the plots. Similar to the AZ case, the AFM state is always semiconducting, while the FM state can be metallic in some structures. Most ZA-GNWs are metallic in their PM state, but structures with large P_Z present a wider band-gap. This is due to the fact that the outer edge for zigzag sectors is short for wide parallel blocks so that the electronic properties are dominated by the semiconducting armchair oblique sectors.

B. Electronic structure of the FM state

Similar to the AZ case, the FM state is the only one to present non-degenerate spin-up and -down bands. We can classify the general features of the bands close to E_F in a similar fashion as we did for AZ-GNWs. This classification is shown in Fig. 8b. In most of the semiconducting cases, the valence band (majority spins) pushes the conductor band (minority spins) to higher energies.

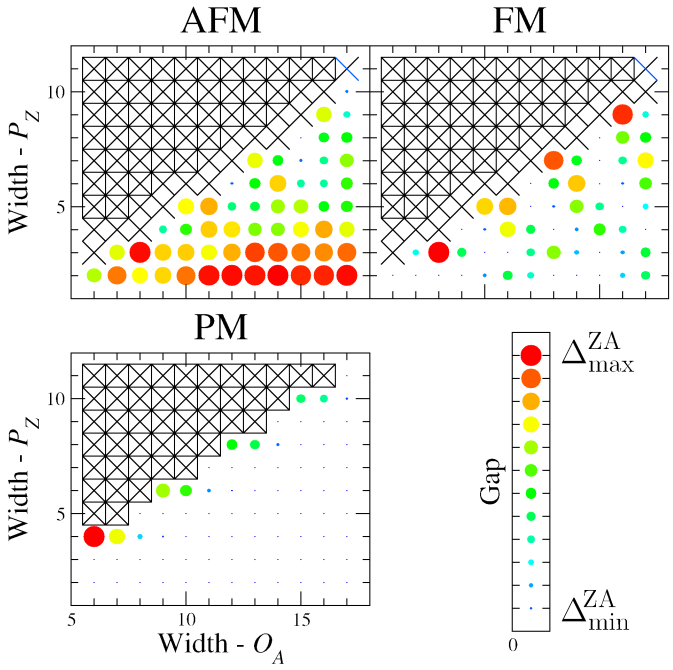

FIG. 11. (color online) Energy band-gap as a function of P and O widths for the multi-magnetic states in ZA-GNWs. Systems that do not possess a stable AFM or FM distribution of spins are marked by a cross, while points marked with a cross inside a square correspond to geometries not allowed by the particular choice for the lengths of the P and O sectors. The minimum and maximum values for the gap in each plot are 107 meV and 477 meV for the AFM state, 0 and 360 meV for FM and 0 and 1527 meV for PM.

C. Band-structure energy

Moving to the systematic study on the band-structure energy, we observe, in general, the following order AFM<FM<PM regarding band-structure energy stability. The values for $|\Delta E|_{max}$ are listed in Table III. The PM state energy is remarkably higher than the other two states for an intermediate parallel width between the minimum and maximum values of P_Z, especially for wider oblique sectors. This is the result of two different factors. First, for narrow parallel sectors, the zigzag edges at opposite sides of the GNW are close to each other, which lowers the magnetic instability of the paramagnetic state[17]. On the other hand, wide P_Z sectors present shorter zigzag edges for a given O_A, thus lowering the instability associated with the PM state. These two opposite trends balance exactly for some value of P_Z where the PM instability reaches its maximum value for a given oblique width (with $O_A \approx 3$ or 4). When comparing FM and AFM, we see that narrower P_Z blocks produce a higher AFM-FM splitting similar to Z-GNRs[17] since the zigzag edges from opposite GNW's sides are closer to each other.

TABLE III. Maximum values of the band-structure energy difference ($|\Delta E|_{max}$) for the different pairs of magnetic states in ZA-GNWs.

$\|\Delta E\|_{max}$ (eV)	PM-AFM	PM-FM	FM-AFM
PM	3.357	2.860	0.993

VII. ELECTRONIC STRUCTURE AND MAGNETIC STATES OF ZZ-GNWS

A. Electronic band-gap

We carried out the systematic study for ZZ-GNWs by varying P_Z and O_Z from 4 to 17. While the particular $(7_Z, 7_Z)$ structure studied in Ref. 25 presented only the PM, AFM and the PM-looking LFiM states, we found out

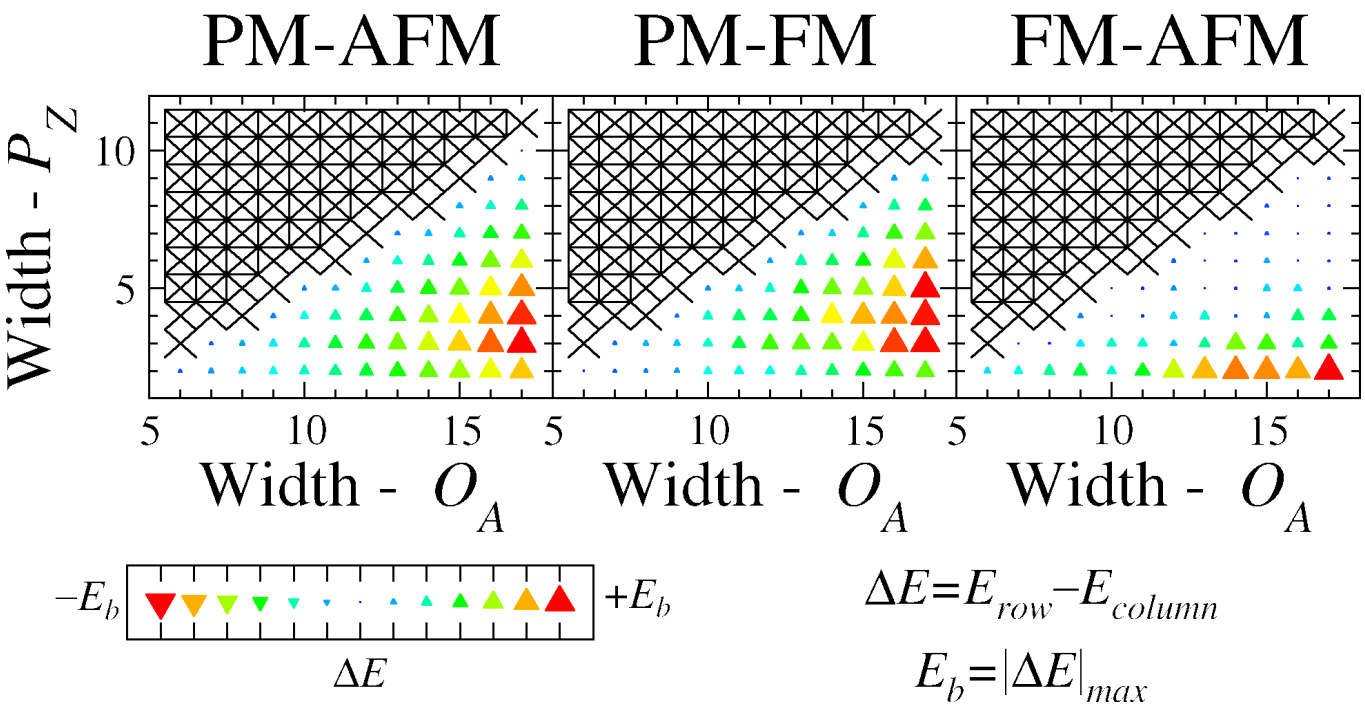

FIG. 12. (color online) Band-structure energy difference among the different magnetic states as a function of P_Z and O_A for ZA-GNWs. Systems that do not possess a stable AFM or FM distribution of spins are marked by a cross, while points marked with a cross inside a square correspond to geometries not allowed by the particular choice for the lengths of the P and O sectors. The $|\Delta E|_{max}$ values for the different plots are shown in Table III.

that other ZZ-GNWs can present the PM state and up to four other spin configurations: AFM, LFiM, FM and TAFM. These distributions are schematically represented in Fig. 5. In Fig. 13 we show the electronic band-gap for all these magnetic states as a function of both P_Z and O_Z. Note that, as it was the case for the $(7_Z, 7_Z)$ system, some structures do not accommodate all these distributions, especially the narrowest structures in the bottom-left part of each plot. Here we choose not to consider the magnetic states where the maximum magnitude of the difference $\langle n_i^{up}\rangle - \langle n_i^{down}\rangle$ (considering all the atoms i in the structure) is less than 0.01. In these plots we used the same values for the Δ_{min}^{ZZ} and Δ_{max}^{ZZ} pair for all the magnetic states, namely $\Delta_{min}^{ZZ} = 0$ and $\Delta_{max}^{ZZ} = 0.45$ eV. To analyze the data, we found convenient to define four different regions on the P_Z–O_Z–gap plot as shown in Fig. 13: (I) bottom-left, (II) upper-left, (III) bottom and (IV) diagonal regions. The narrowest structures are in (I), where we find most of the structures with missing magnetic states since narrow structures have a reduced paramagnetic instability[17]. Region (II) is characterized by structures whose outer parallel edge is short enough so that this edge does not present significant spin polarization. In this case we observe that the AFM and TAFM states are similar to each other, while we note the same for the FM and LFiM states. A similar picture can be drawn in region (III) as the structures over this region present short oblique edges where the spin polarization does not reach significant values. One observes that the plots over regions (II) and (III) are practically the same for the AFM-TAFM and FM-LFiM pairs. The main differences reside on region (IV) where the wide structures present a high value for the paramagnetic instability, allowing spin polarization along all the edges on the ZZ-GNW.

For all magnetic states, we observe that the combined variations along the horizontal and vertical directions explain why the gap tends to get smaller along the chart's diagonal (to eventually vanish as the 2D graphene character is progressively recovered).

B. Electronic structure of the FM and LFiM states

For ZZ-GNWs, both the FM and LFiM states break the spin up-down symmetry and present non zero total magnetization so that we observe different bands for spin-up and -down states. Classifying the electronic bands features around the Fermi energy as in the case of AZ- and ZA-GNWs, we obtain the schemes plotted in Figs. 8c-d. We note that, contrary to the AZ-GNWs case, the systems with metallic behavior are spread along the entire $P_Z - O_Z$ plane, even though they are more concentrated on the $P_Z \geq O_Z$ part of the plot for the FM state. In addition, we

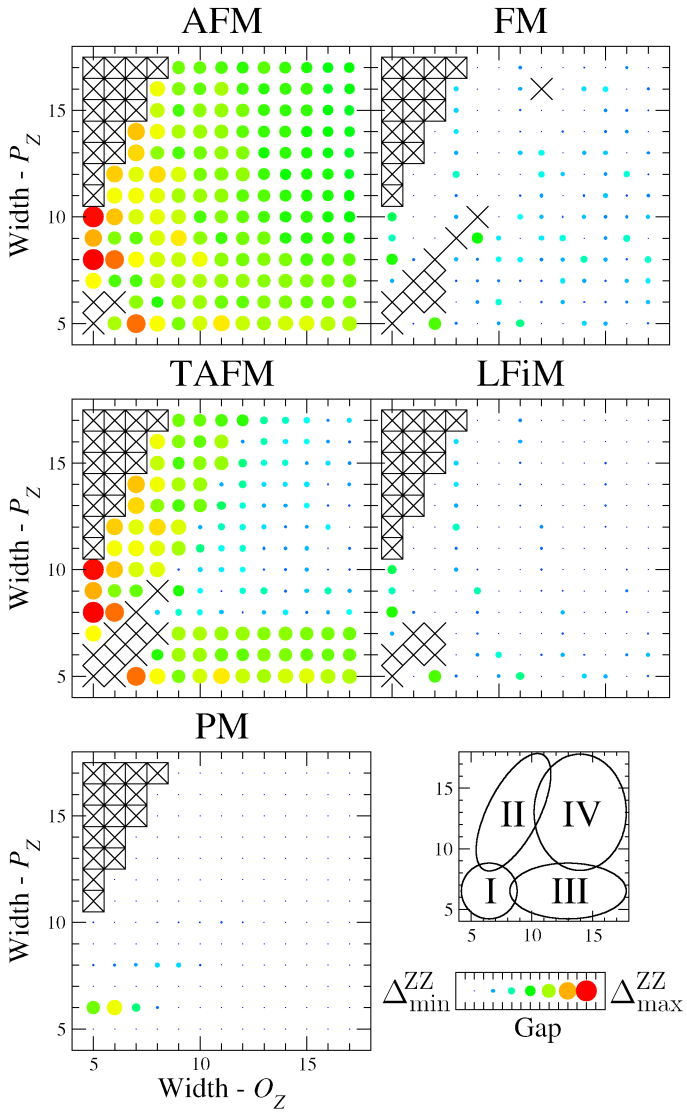

FIG. 13. (color online) Energy band-gap as a function of P_Z and O_Z widths for the multi-magnetic states in ZZ-GNWs. Systems that do not possess a stable AFM, TAFM, LFiM or FM distribution of spins are marked by a cross, while points marked with a cross inside a square correspond to geometries not allowed by the particular choice for the lengths of the P and O sectors. The minimum and maximum gap values are $\Delta^{ZZ}_{min} = 0$ and $\Delta^{ZZ}_{max} = 0.45$ eV, respectively.

observe that the LFiM state has a more pronounced tendency to behave as a metal as can be seen by the dominant number of stars in Fig. 8d (or by the large number of small blue circles on the LFiM-gap-plot from Fig. 13). We also note that most semiconducting structures in the FM state have their highest band below E_F corresponding to the majority spin. However, in the LFiM case, there is no dominant tendency to present S $\uparrow\downarrow$ or S $\downarrow\uparrow$ bands as we have zigzag edges with different majority spin within the same unit cell.

C. Band-structure energy

In Fig. 14, we plot the TBU band-structure energy difference for different pairs of states (the values for $|\Delta E|_{max}$ in each case are shown in Table IV). The PM-AFM energy difference is plotted in the lower right plot of Fig. 14. We observe that the energy separation for these two states is always positive (in other words, AFM is always more stable) and increases as we move away from region (I) in the plot. This is a clear manifestation of the increasing (lowering) of the paramagnetic instability as the system gets wider (narrower) in either parallel or oblique sectors or

in both. We observe the same features for the PM-X (X=FM, LFiM, TAFM) energy difference. Moving to the other cases, regions (II) and (III) in the plots for the TAFM-AFM and FM-LFiM differences are predominantly dark blue dots (corresponding to $\Delta E \to 0$), as expected from the early discussion on the band-gap. Finally, now focusing on region (IV), we note an overall PM>FM>TAFM>LFiM>AFM energetic order for the magnetic states (except for some points in the FM-TAFM plot).

TABLE IV. Maximum values of the band-structure energy difference ($|\Delta E|_{max}$) for the different pairs of magnetic states in ZZ-GNWs.

$\lvert\Delta E\rvert_{max}$ (eV)	AFM	LFiM	TAFM	FM
PM	6.014	5.872	5.373	5.364
FM	0.851	0.658	0.623	–
TAFM	0.872	0.638	–	–
LFiM	0.474	–	–	–

VIII. CONCLUSIONS

We presented a systematic study of the electronic properties of all three achiral classes of GNWs containing at least one zigzag edged sector. We described a detailed framework to determine the GNW's structure using a reduced set of parameters and studied the details of the electronic structure of each GNW class. While non-spin-polarized Z-GNRs present a high electron density along the edges[17] which can be further stabilized through the formation of AFM and FM states, GNWs allow the formation of a larger variety of magnetic states due to the segmented edge configuration from these wiggles. Most important, we show that even though we can describe GNWs in terms of their A- and Z-GNRs building blocks, their properties cannot be simply reduced to a simple juxtaposition of the properties of their GNR components. In fact, the details of the parallel and oblique sectors assembly, as well as the corresponding spin distributions, can result in completely different behaviors for the GNWs electronic structure which have no counterparts in GNRs. As a result, these structures present a broader and richer set of physical properties compared with their constituent GNRs.

Once experimental control over these magnetic states is achieved, GNWs have the potential to constitute prototype materials for a series of nanoelectronic and spintronic applications as they allow the manipulation of the system's electronic properties by means of the electronic spin. Hence, we expect that optical and electronic transport properties to be fine tuned not only by changes in the atomic structure, but also by selecting the magnetic state, allowing a single structure to present multiple physical behaviors by changing its spin distribution and increasing the number of available mechanisms to control the flow of charges.

IX. ACKNOWLEDGEMENTS

E. C. G. acknowledges the Brazilian agencies CAPES for the sandwich program fellowship (process 0327-10-7) and CNPq (process 140887/2008-3). E. C. S. was supported in part by PHASE, an EFRC funded by the US-DOE under Award Number DE-SC0001087. A. G. S. F. acknowledges support from CNPq and NANOBIOSIMES institute. V. M. was partially supported by an appointment to the HERE program for faculty at the Oak Ridge National Laboratory (ORNL) administered by ORISE and by New York State under NYSTAR contract C080117. All the calculations were performed on resources from the Computational Center for Nanotechnology Innovation at RPI.

Appendix A: Lattice parameter

Here we provide details on how to determine geometrical properties of the various types of GNWs from their defining parameters. We start with the lattice parameter, followed by the number of atoms in a GNW's unit cell.

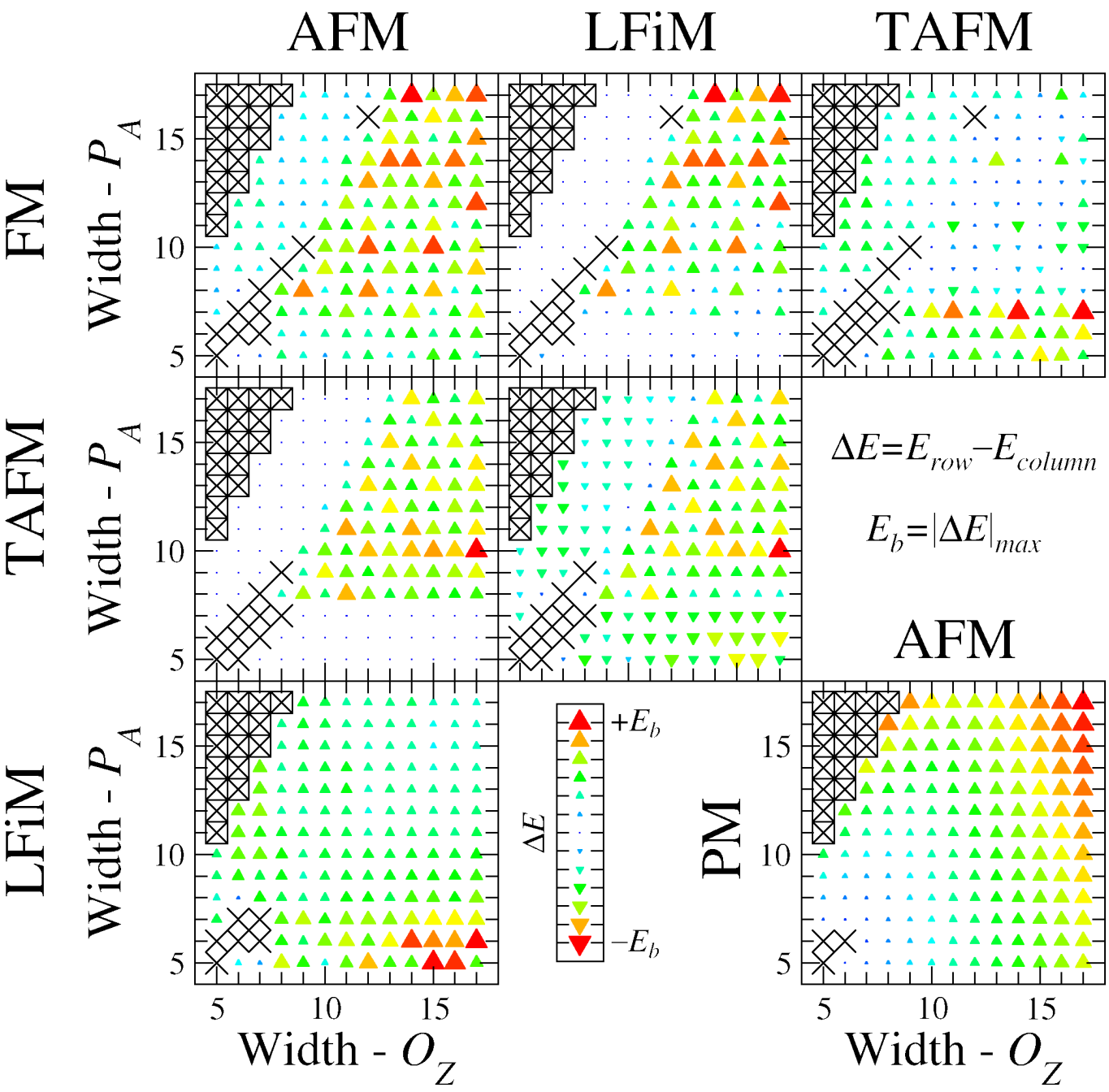

FIG. 14. (color online) Band-structure energy difference among the different magnetic states as a function of P_Z and O_Z in ZZ-GNWs. Systems that do not possess a stable AFM, TAFM, LFiM or FM distribution of spins are marked by a cross, while points marked with a cross inside a square correspond to geometries not allowed by the particular choice for the lengths of the P and O sectors. The $|\Delta E|_{max}$ values for the different plots are shown in Table IV.

1. General approach

In order to determine the unit cell length $\mathcal{L}$ of a GNW as a function of W_p, L_p, W_o and L_o, we define the set $(b, c, d, e, h, l, w, x, y)$ of characteristic lengths for a general GNW unit cell as in Fig. 15. The angle θ is either 60° (for AA- and ZZ-GNWs) or 30° (for AZ- and ZA-GNWs). In this figure we define the limits of the blue shaded area as being the lines containing the frontier carbon atoms from the wiggle.

From Fig. 15, we see that the lattice constant $\mathcal{L}$ for the GNW unit cell is given by:

$$\mathcal{L} = x + y. \tag{A1}$$

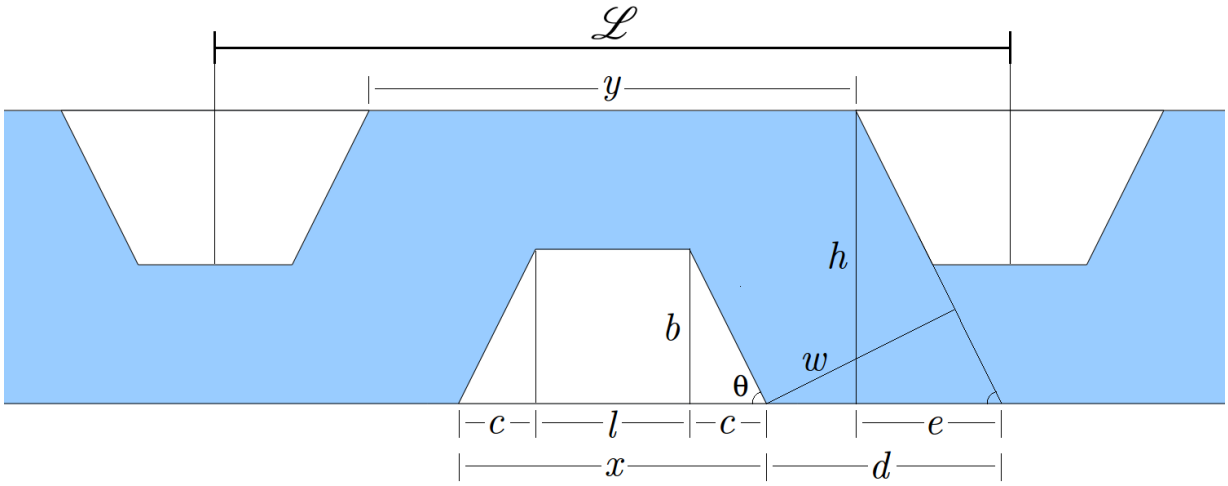

FIG. 15. Auxiliary lengths to determine the lattice parameter of a general GNW unit cell.

We can also write:

$$x = l + 2c \qquad \text{and} \qquad c = b/\tan\theta \tag{A2}$$

as well as:

$$y = 2d + x - 2e; \qquad d = w/\sin\theta \qquad e = h/\tan\theta \tag{A3}$$

so that:

$$\mathcal{L} = \frac{2w}{\sin\theta} + 2l + \frac{4b}{\tan\theta} - \frac{2h}{\tan\theta}. \tag{A4}$$

Depending on the values for w, l, b, h and θ, we have different equations for each type of GNW.

2. The l length

By definition, l is trivially determined for AA- and AZ-GNWs by:

$$l = L_p a_{CC}. \tag{A5}$$

A careful observation of the ZA-GNW structures (see, e. g., Fig. 16a) allows us to write l for the ZA case as the distance between the two ending zigzag tips on the wedge's parallel edge:

$$l = (L_p - 1)a \tag{A6}$$

while we have to add a length $2f$ (defined in Fig. 16b) to this last result to obtain the corresponding length for the ZZ case. The value of f is easily obtained with the help of Fig. 16b as:

$$f = a - \frac{a_{CC}/2}{\cos 30^\circ} = \frac{2a}{3} \tag{A7}$$

so that

$$l = (L_p + \frac{1}{3})a. \tag{A8}$$

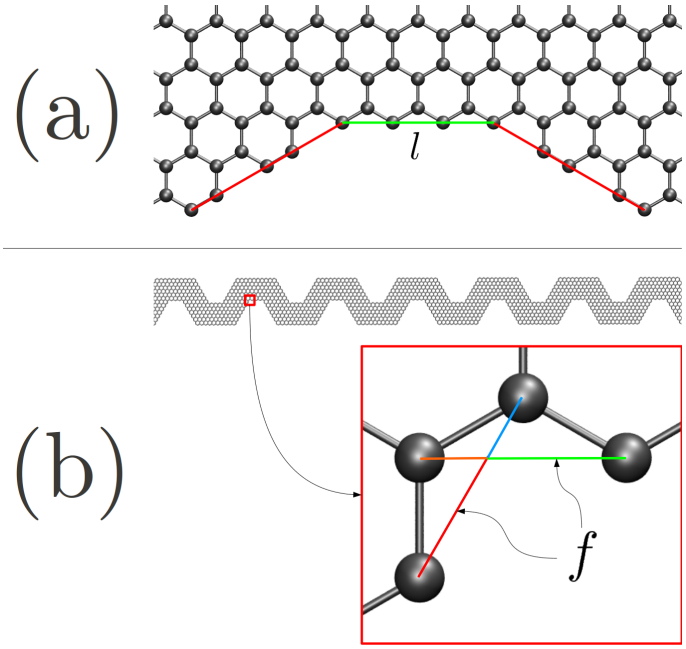

FIG. 16. Auxiliary length l for ZA-GNWs (a) and increment f for ZZ-GNWs (b).

3. The w, h and b lengths

As a set of n $C-C$ parallel lines in graphene is $(n-1)a/2$ wide (where $a = a_{CC}\sqrt{3}$) and the width for a set of n zigzag strips is $(3n-2)a_{CC}/2$, w is expressed as:

$$w = \frac{(W_o - 1)a}{2} \qquad \text{for AA- and ZA-GNWs} \tag{A9}$$

$$w = \frac{(3W_o - 2)a_{CC}}{2} \qquad \text{for AZ- and ZZ-GNWs.} \tag{A10}$$

For the same reason we can write h as:

$$h = \frac{(L_o - 1)a}{2} \qquad \text{for AA- and AZ-GNWs} \tag{A11}$$

$$h = \frac{(3L_o - 2)a_{CC}}{2} \qquad \text{for ZA- and ZZ-GNWs} \tag{A12}$$

and finally b is obtained by:

$$b = h - \frac{(W_p - 1)a}{2} = \frac{(L_o - W_p)a}{2} \qquad \text{for AA- and AZ-GNWs} \tag{A13}$$

$$b = h - \frac{(3W_p - 2)a_{CC}}{2} = \frac{3(L_o - W_p)a_{CC}}{2} \qquad \text{for ZA- and ZZ-GNWs.} \tag{A14}$$

4. Lattice parameter relations

With the previous results it is trivial to write:

$$\mathcal{L}_{AA} = (2W_o + L_o + 2L_p - 2W_p - 1)a_{CC} \tag{A15}$$

$$\mathcal{L}_{AZ} = (6W_o + 3L_o + 2L_p - 6W_p - 1)a_{CC} \tag{A16}$$

$$\mathcal{L}_{ZA} = (2W_o + 3L_o + 2L_p - 6W_p - 2)a_{CC}\sqrt{3} \tag{A17}$$

$$\mathcal{L}_{ZZ} = (2W_o + L_o + 2L_p - 2W_p)a_{CC}\sqrt{3}. \tag{A18}$$

Appendix B: Number of atoms

In order to determine how many atoms ($\mathcal{N}$) are contained within a GNW's unit cell we first calculate the area corresponding to the wedge-healed GNW. We then carve out the area from the trapezoidal wedges and divide the result by the area of half hexagon. Observe that the non-parallel sides and the smallest basis from these trapezoids are positioned half way between the corresponding sides on the trapezoids composed by the GNW's edge atoms and the edge atoms from the removed graphene flakes (as depicted in Fig. 17). An analogous definition is made for the lines determining the limits of the healed ribbon. The important quantities to determine are shown in Fig. 17. With

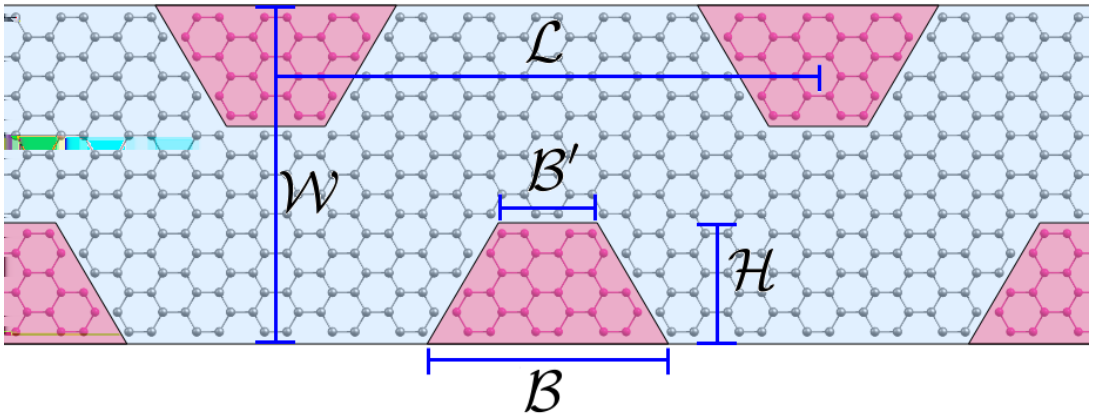

FIG. 17. Auxiliary lengths used to determine the number $\mathcal{N}$ of atoms in a GNW's unit cell.

these definitions we can write:

$$\mathcal{N} = \Big(\mathcal{L}\mathcal{W} - (\mathcal{B}+\mathcal{B}')\mathcal{H}\Big)/(3a_{CC}a/4) \tag{B1}$$

where $\mathcal{L}$ is the length of the GNW's unit cell (determined in the last section), $\mathcal{W}$ is the healed GNW's width, $\mathcal{H}$ is the height of the deleted trapezoids and $\mathcal{B}$ and $\mathcal{B}'$ are, respectively the largest and smallest basis from the trapezoids. Again, we have specific results for each GNW kind.

1. Healed GNW's width $\mathcal{W}$ and wedge's height $\mathcal{H}$

Based on the considerations from Section A 3 we can write $\mathcal{W}$ as:

$$\mathcal{W} = L_o a/2 \qquad \text{for AA- and AZ-GNWs} \tag{B2}$$
$$\mathcal{W} = 3L_o a_{CC}/2 \quad \text{for ZA- and ZZ-GNWs,} \tag{B3}$$

where we added $a/2$ in the first case and a_{CC} in the second since the lines defining the limits of the healed GNW's area are located half way between the GNR frontier atoms and those from the carved graphene structure. In a similar way, we derive the following expressions for $\mathcal{H}$:

$$\mathcal{H} = (L_o - W_p)a/2 \qquad \text{for AA- and AZ-GNWs} \tag{B4}$$
$$\mathcal{H} = 3(L_o - W_p)a_{CC}/2 \quad \text{for ZA- and ZZ-GNWs.} \tag{B5}$$

2. Wedge's basis $\mathcal{B}$ and $\mathcal{B}'$

Consider the trapezoid formed by the lines passing through the frontier atoms from the deleted trapezoidal flakes. Let l' and l'' be the smallest and largest basis from this trapezoid. For AA- and AZ-GNWs this value is $l' = l - a_{CC}$. So $\mathcal{B}'$ is given by:

$$\mathcal{B}' = \frac{l + l'}{2} = L_p a_{CC} - a_{CC}/2. \tag{B6}$$

For the ZA-GNWs case we have $l' = l$ and:

$$\mathcal{B}' = \frac{l + l'}{2} = (L_p - 1)a. \tag{B7}$$

In ZZ-GNWs we have $l' = l - f$ and:

$$\mathcal{B}' = \frac{l + l'}{2} = L_p a. \tag{B8}$$

In order to obtain $\mathcal{B}$ we also consider the trapezoid defined by the frontier atoms from 2D graphene after carving out the trapezoidal flakes. Let l''' be the largest basis from this trapezoid. For AA-GNWs we have $l'' = l + 2c - 2a_{CC}$ and $l''' = l + 2c + a_{CC}$ so that:

$$\mathcal{B} = \frac{l'' + l'''}{2} = (L_p + L_o - W_p - \frac{1}{2})a_{CC} \tag{B9}$$

For AZ-GNWs we have $l'' = l + 2c - 4a_{CC}$ and $l''' = l + 2c + 3a_{CC}$ so that:

$$\mathcal{B} = \frac{l'' + l'''}{2} = (L_p + 3L_o - 3W_p - \frac{1}{2})a_{CC} \tag{B10}$$

Moving to ZA-GNWs, we have $l'' = l + 2c - 2a$ and $l''' = l + 2c + 2a$ and:

$$\mathcal{B} = \frac{l'' + l'''}{2} = (L_p + 3L_o - 3W_p - 1)a. \tag{B11}$$

Finally, ZZ-GNWs are such that $l'' = l + 2c - 2f$ and $l''' = l + 2c + a$, resulting in:

$$\mathcal{B} = \frac{l'' + l'''}{2} = (L_p + L_o - W_p)a \tag{B12}$$

3. Formulas for $\mathcal{N}$

The previous results allow us to write

$$\mathcal{N}_{ZZ} = 4W_o L_o + 4L_p W_p - 2W_p^2 \tag{B13}$$
$$\mathcal{N}_{ZA} = 4W_o L_o + 4L_p W_p - 6W_p^2 - 4W_p \tag{B14}$$
$$\mathcal{N}_{AZ} = (12W_o L_o + 4L_p W_p - 6W_p^2 - 2W_p)/3 \tag{B15}$$
$$\mathcal{N}_{AA} = (4W_o L_o + 4L_p W_p - 2W_p^2 - 2W_p)/3. \tag{B16}$$

4. Corrections on the AA-GNW case

Note that Eq. B16 does not provide the correct result in all the cases. The reason is that when calculating the area from the two trapezoids, we are actually calculating the area of a parallelogram composed by the two trapezoids in a construction similar to that shown in Fig. 18a,b. However, the simple superposition of the two trapezoids may not be compatible with the bonds made by the carbon atoms depending on the defining parameters of the GNW. By simple observation, the superposition of the two trapezoids is correct when:

- $mod(L_p, 3) = 2$ and $mod(L_o - W_p, 3) = 0$ (see example in Fig. 18a);
- $mod(L_p, 3) = 1$ and $mod(L_o - W_p, 3) = 2$ (see example in Fig. 18b).

The method has to be adapted for the other cases. Let us consider first the case $mod(L_p, 3) = 2$. When $L_o - W_p = 3i + 2$, we should shift each trapezoid in Fig. 18a by $a/2$ (perpendicular to their basis, one up and the other down), in such a way that the smallest line of $C - C$ bonds get out of the parallelogram (see example in Fig. 18c). So, the deleted atoms are composed by those inside the new parallelogram plus the atoms in the two $C - C$ lines outside the the parallelogram ($2(L_p + 1)/3$ in each). The part of each trapezoid included in the parallelogram has a smallest basis a_{CC} larger and a height $a/2$ shorter. Thus, the number of atoms will be given by:

$$\mathcal{N}_{AA} = (4W_o L_o + 4L_p W_p - 2W_p^2 - 2W_p - 4)/3. \tag{B17}$$

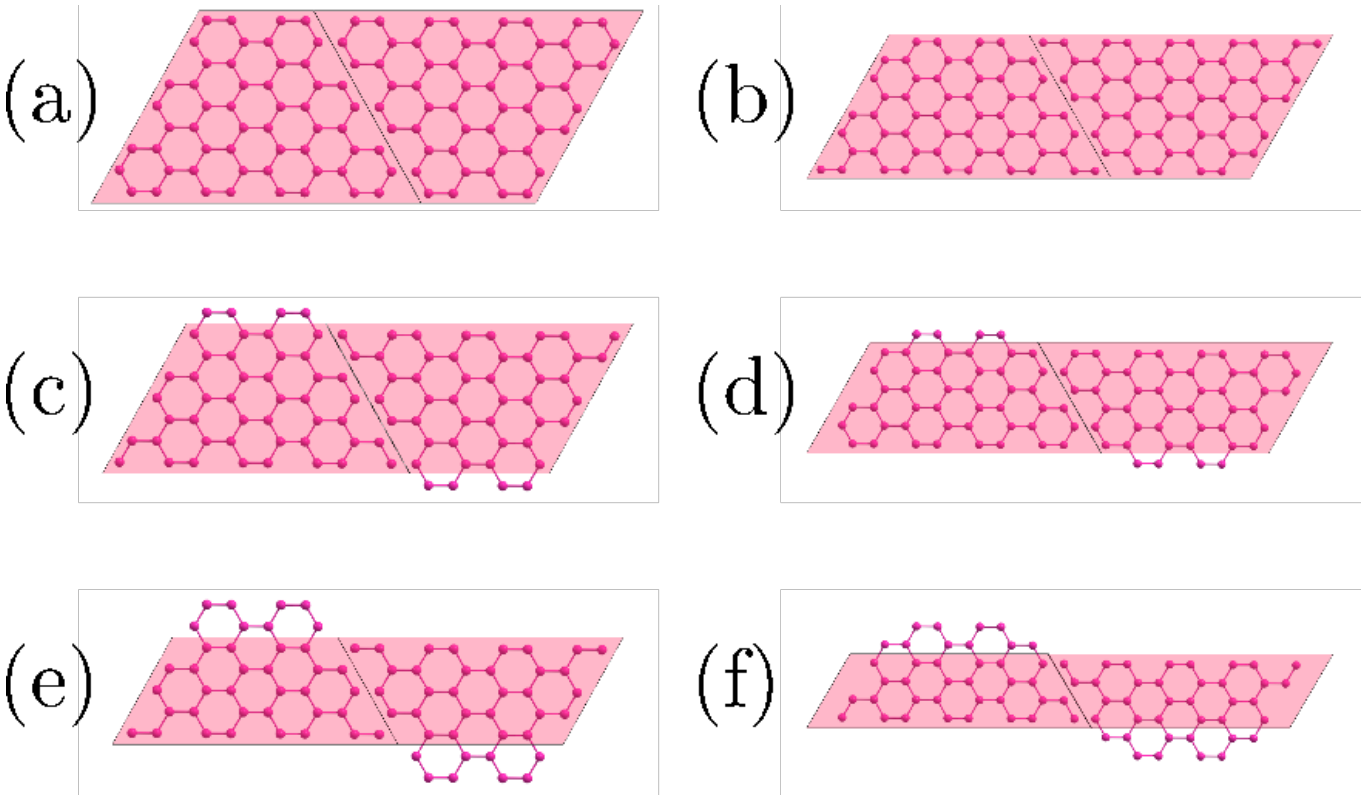

FIG. 18. Auxiliary scheme to calculate the number of deleted atoms in a GNW's wedge.

When $L_o - W_p = 3i + 1$, we should shift each trapezoid in Fig. 18a by a (perpendicular to their basis, one up and the other down), in such a way that the two smallest lines of $C - C$ bonds get out of the parallelogram (see example in Fig. 18e). It follows that the removed atoms are composed by those inside the new parallelogram plus the atoms in the four $C - C$ lines outside the parallelogram ($2(L_p + 1)/3$ in each). The part of each trapezoid included in the parallelogram has a smallest basis $2a_{CC}$ bigger and a height a shorter. So, the number of atoms will be given by:

$$\mathcal{N}_{AA} = (4W_oL_o + 4L_pW_p - 2W_p^2 - 2W_p - 4)/3. \tag{B18}$$

Let us now consider the case $mod(L_p, 3) = 1$. When $L_o - W_p = 3i + 1$, we should shift each trapezoid in Fig. 18b by $a/2$ (perpendicular to their basis, one up and the other down), in such a way that the smallest line of $C - C$ bonds get out of the parallelogram (see example in Fig. 18d). Therefore, the deleted atoms are composed by those inside the new parallelogram plus the atoms in the two $C - C$ lines outside the parallelogram ($2(L_p - 1)/3$ in each). The part of each trapezoid included in the parallelogram has a longer smallest basis (a_{CC} longer) and a shorter height ($a/2$ shorter). So, the number of atoms will be given by:

$$\mathcal{N}_{AA} = (4W_oL_o + 4L_pW_p - 2W_p^2 - 2W_p + 4)/3. \tag{B19}$$

When $L_o - W_p = 3i$, we should shift each trapezoid in Fig. 18b by a (perpendicular to their basis, one up and the other down), in such a way that the two smallest lines of $C - C$ bonds get out of the parallelogram (see example in Fig. 18f). The deleted atoms are therefore defined by those inside the new parallelogram plus the atoms in the four $C - C$ lines outside the parallelogram ($2(L_p - 1)/3$ in each of the smallest two and $2 + 2(L_p - 1)/3$ in each of the others). The part of each trapezoid included in the parallelogram has a smallest basis which is $2a_{CC}$ larger and a height being a shorter. Therefore, the number of atoms will be given by:

$$\mathcal{N}_{AA} = (4W_oL_o + 4L_pW_p - 2W_p^2 - 2W_p)/3 \tag{B20}$$

so that the downsizing on the trapezoids area and the addition of the two lines of atoms compensate each other so that we end up with the same formula as for the cases exemplified in Fig. 18a-b.

In addition, examination of Fig. 18c,f reveals that we have to subtract 4 atoms when $mod(L_p, 3) = mod(L_o - W_p) = 2$ or $mod(L_p, 3) = 1$ and $mod(L_o - W_p) = 0$ to eliminate four single bonded atoms at the corners of the outer parallel edges.

[1] K. Novoselov, A. Geim, S. Morozov, D. Jiang, Y. Zhang, S. Dubonos, I. Grigorieva, A. Firsov. *Science* **306**(5696), 666 (2004).
[2] R. Van Noorden. *Nature* **469**(7328), 14 (2011).
[3] C.-A. Palma, P. Samori. *Nature Chemistry* **3**(6), 431 (2011).
[4] L. A. Ponomarenko, F. Schedin, M. I. Katsnelson, R. Yang, E. W. Hill, K. S. Novoselov, A. K. Geim. *Science* **320**(5874), 356 (2008).
[5] M. Y. Han, B. Özyilmaz, Y. Zhang, P. Kim. *Phys. Rev. Lett.* **98**, 206805 (2007).
[6] L. Tapaszto, G. Dobrik, P. Lambin, L. P. Biro. *Nature Nanotechnology* **3**(7), 397 (2008).
[7] X. Wang, H. Dai. *Nature Chemistry* **2**(8), 661 (2010).
[8] R. Yang, L. Zhang, Y. Wang, Z. Shi, D. Shi, H. Gao, E. Wang, G. Zhang. *Advanced Materials* **22**(36), 4014 (2010).
[9] L. Xie, L. Jiao, H. Dai. *Journal of the American Chemical Society* **132**(42), 14751 (2010).
[10] D. V. Kosynkin, A. L. Higginbotham, A. Sinitskii, J. R. Lomeda, A. Dimiev, B. K. Price, J. M. Tour. *Nature* **458**(7240), 872 (2009).
[11] L. Jiao, L. Zhang, X. Wang, G. Diankov, H. Dai. *Nature* **458**(7240), 877 (2009).
[12] M. Bieri, M.-T. Nguyen, O. Groening, J. Cai, M. Treier, K. Ait-Mansour, P. Ruffieux, C. A. Pignedoli, D. Passerone, M. Kastler, K. Muellen, R. Fasel. *Journal of the American Chemical Society* **132**(46), 16669 (2010).
[13] L. Grill, M. Dyer, L. Lafferentz, M. Persson, M. V. Peters, S. Hecht. *Nature Nanotechnology* **2**(11), 687 (2007).
[14] J. Lu, P. S. E. Yeo, C. K. Gan, P. Wu, K. P. Loh. *Nature Nanotechnology* **6**(4), 247 (2011).
[15] L. Lafferentz, F. Ample, H. Yu, S. Hecht, C. Joachim, L. Grill. *Science* **323**(5918), 1193 (2009).
[16] J. Cai, P. Ruffieux, R. Jaafar, M. Bieri, T. Braun, S. Blankenburg, M. Muoth, A. P. Seitsonen, M. Saleh, X. Feng, K. Muellen, R. Fasel. *Nature* **466**(7305), 470 (2010).
[17] L. Pisani, J. A. Chan, B. Montanari, N. M. Harrison. *Physical Review B* **75**(6), 064418 (2007).
[18] Y.-W. Son, M. L. Cohen, S. G. Louie. *Physical Review Letters* **97**(21), 216803 (2006).
[19] Y.-W. Son, M. L. Cohen, S. G. Louie. *Nature* **444**(7117), 347 (2006).
[20] A. Saffarzadeh, R. Farghadan. *Applied Physics Letters* **98**(2), 023106 (2011).
[21] Z. F. Wang, Q. W. Shi, Q. Li, X. Wang, J. G. Hou, H. Zheng, Y. Yao, J. Chen. *Applied Physics Letters* **91**(5), 053109 (2007).
[22] Y. Hancock, K. Saloriutta, A. Uppstu, A. Harju, M. J. Puska. *Journal of Low Temperature Physics* **153**(5-6), 393 (2008).
[23] H. Sevincli, M. Topsakal, S. Ciraci. *Physical Review B* **78**(24), 245402 (2008).
[24] M. Topsakal, H. Sevincli, S. Ciraci. *Applied Physics Letters* **92**(17), 173118 (2008).
[25] E. C. Girão, L. Liang, E. Cruz-Silva, A. G. Souza Filho, V. Meunier. *Physical Review Letters* **107**, 135501 (2011).
[26] S. S. Datta, D. R. Strachan, S. M. Khamis, A. T. C. Johnson. *Nano Letters* **8**(7), 1912 (2008).
[27] Y. Chen, T. Jayasekera, A. Calzolari, K. W. Kim, M. B. Nardelli. *Journal of Physics-Condensed Matter* **22**(37) (2010).
[28] W. Huang, J.-S. Wang, G. Liang. *Physical Review B* **84**(4) (2011).
[29] J. Fernández-Rossier, J. J. Palacios. *Physical Review Letters* **99**, 177204 (2007).
[30] J. Fernández-Rossier. *Physical Review B* **77**, 075430 (2008).
[31] O. Hod, V. Barone, G. E. Scuseria. *Physical Review B* **77**, 035411 (2008).
[32] E. Cruz-Silva, Z. M. Barnett, B. G. Sumpter, V. Meunier. *Physical Review B* **83**, 155445 (2011).
[33] T. G. Pedersen, C. Flindt, J. Pedersen, N. A. Mortensen, A.-P. Jauho, K. Pedersen. *Physical Review Letters* **100**(13), 136804 (2008).
[34] J. J. Palacios, J. Fernández-Rossier, L. Brey. *Physical Review B* **77**, 195428 (2008).
[35] P. Simonis, C. Goffaux, P. Thiry, L. Biro, P. Lambin, V. Meunier. *Surface Science* **511**(1-3), 319 (2002).
[36] A. R. Botello-Mendez, X. Declerck, M. Terrones, H. Terrones, J. C. Charlier. *Nanoscale* **3**(7), 2868 (2011).
[37] A. R. Botello-Mendez, E. Cruz-Silva, J. M. Romo-Herrera, F. Lopez-Urias, M. Terrones, B. G. Sumpter, H. Terrones, J. C. Charlier, V. Meunier. *Nano Letters* **11**(8), 3058 (2011).
[38] O. V. Yazyev, S. G. Louie. *Nature Materials* **9**(10), 806 (2010).
[39] Z. Ma, W. Sheng. *Applied Physics Letters* **99**(8), 083101 (2011).
[40] O. V. Yazyev. *Reports on Progress in Physics* **73**(5), 056501 (2010).
[41] M. Milnera, J. Kürti, M. Hulman, H. Kuzmany. *Physical Review Letters* **84**(6), 1324 (2000).
[42] R. Saito, G. Dresselhaus, M. S. Dresselhaus. *Physical Review B* **61**(4), 2981 (2000).
[43] D. Gunlycke, C. T. White. *Physical Review B* **77**, 115116 (2008).
[44] O. V. Yazyev. *Nano Letters* **8**(4), 1011 (2008).
[45] J. Fischer, B. Trauzettel, D. Loss. *Physical Review B* **80**, 155401 (2009).
[46] O. Hod, J. E. Peralta, G. E. Scuseria. *Physical Review B* **76**, 233401 (2007).
[47] D. en Jiang, S. Dai .
[48] E. H. Lieb. *Physical Review Letters* **62**, 1201 (1989).
[49] E. Anderson, Z. Bai, C. Bischof, S. Blackford, J. Demmel, J. Dongarra, J. Du Croz, A. Greenbaum, S. Hammarling, A. McKenney, D. Sorensen. *LAPACK Users' Guide*. Society for Industrial and Applied Mathematics, Philadelphia, PA, third ed. (1999).
[50] P. Pulay. *Chemical Physics Letters* **73**(2), 393 (1980).
[51] M. Pan, E. C. Giro, X. Jia, S. Bhaviripudi, Q. Li, J. Kong, V. Meunier, M. S. Dresselhaus. *Nano Letters* **12**(4), 1928 (2012).

[52] K. Wakabayashi, M. Fujita, H. Ajiki, M. Sigrist. *Physical Review B* **59**(12), 8271 (1999).